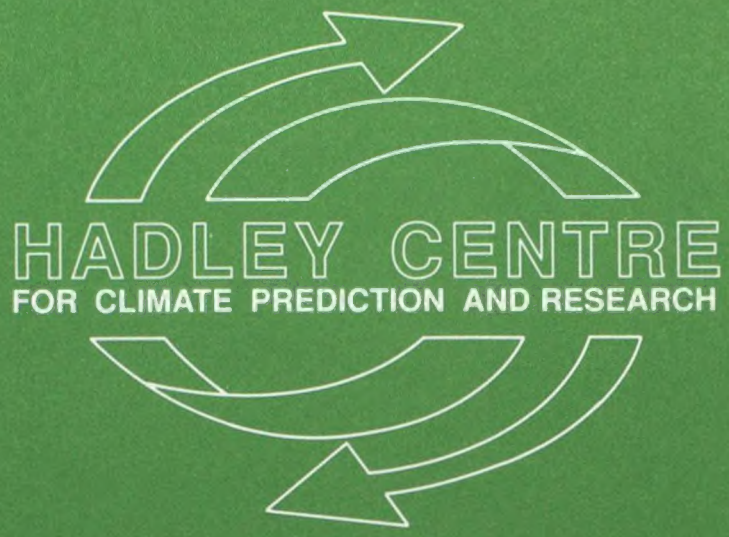

Simulation of clear-sky outgoing longwave radiation over the oceans using operational analyses.

by

A. Slingo and M. J. Webb

CRTN 31 July 1992

CLIMATE
RESEARCH
TECHNICAL
NOTE

Hadley Centre
Meteorological Office
London Road
Bracknell
Berkshire RG12 2SY

CLIMATE RESEARCH TECHNICAL NOTE NO. 31

SIMULATION OF CLEAR-SKY OUTGOING LONGWAVE RADIATION OVER THE OCEANS USING OPERATIONAL ANALYSES

by

A SLINGO and M J WEBB

To be published in the October 1992 issue of the
Quarterly Journal of the Royal Meteorological Society

Hadley Centre for Climate Prediction and Research
Meteorological Office
London Road
Bracknell
Berkshire RG12 2SY
U.K.

SIMULATION OF CLEAR-SKY OUTGOING LONGWAVE RADIATION OVER THE OCEANS USING OPERATIONAL ANALYSES

A. Slingo and M.J. Webb

Hadley Centre for Climate Prediction and Research, Meteorological Office, Bracknell

(Submitted January 1992, revised May 1992)

Summary

We have developed a system for the Simulation and Analysis of Measurements from Satellites using Operational aNalyses (SAMSON). In this initial study, simulations of clear-sky Outgoing Longwave Radiation (OLR) over the oceans are compared with data from the Earth Radiation Budget Experiment (ERBE). The calculations were performed with a Malkmus narrow-band radiation scheme, including the effects of all the radiatively important gases. Sea surface temperatures were taken from the National Meteorological Center's blended analyses and ozone data from the Nimbus 7 Solar Backscatter Ultraviolet experiment. Atmospheric temperatures and humidities came from operational analyses. Parallel simulations were performed with the analyses produced both by the European Centre for Medium-range Weather Forecasts (ECMWF) and by the United Kingdom Meteorological Office.

Simulations for the period February 1985 to October 1986 are compared with ERBE data. Differences between the humidity data in the analyses have a significant impact on the calculated clear-sky OLR. The changes to the ECMWF model in May 1985 reduce the differences compared with ERBE. After this time, the differences are consistent with two known systematic errors; a small overestimate in the ERBE data and a tendency for the ECMWF analyses to be too dry in the ITCZ and too moist in the sub-tropics. The simulations with the UKMO analyses generally show slightly larger differences compared with ERBE. Tests show the sensitivity of the ECMWF results to diurnal sampling of the analyses and to the temporal resolution employed to calculate the monthly means. These tests reveal instances of extremely low humidities in the ECMWF analyses in the upper troposphere over the tropical East Pacific.

Over most of the domain, the simulations are within 5-10 Wm^{-2} of the ERBE data. The clear-sky OLR can thus be computed from operational analyses with an accuracy comparable with that of ERBE. This indicates the potential of such simulations and has implications for the planning of future radiation budget observations.

1. Introduction

The Earth's Radiation Budget has now been observed by broad-band satellite sensors for more than a decade. These sensors provide information on the two components of the budget; the reflected solar radiation and the emitted thermal radiation at the top of the atmosphere. The longest time series of such data comes from the Nimbus 7 satellite, launched in 1978 (Kyle et al. 1985). The most comprehensive data have been provided since late 1984 by the Earth Radiation Budget Experiment (ERBE), using identical sensors on one research satellite and two operational weather satellites (Barkstrom 1984). An important feature of ERBE is the additional archival of the radiation budget observed under clear-sky conditions. This allows the effect of clouds on the radiation budget to be estimated, by differencing the total and clear-sky data, to produce the 'cloud radiative forcing' diagnostic (Ramanathan et al. 1989, Harrison et al. 1990). The Nimbus 7 clear-sky fluxes were not archived, but estimates of the cloud radiative forcing have been produced by other means (e.g. Ardanuy et al. 1989, Stephens and Greenwald 1991). There is thus a great deal of data now available on the Earth's radiation budget and on the separate contributions from clear and cloudy skies.

In addition to these observations of the radiation budget, data from narrow-band sensors have been processed to give information on cloud amounts and radiative properties. The Nimbus 7 Global Cloud Climatology (Stowe et al. 1989) is derived from infrared radiances and ultraviolet reflectivities measured by different instruments from those which measure the radiation budget on this satellite. The International Satellite Cloud Climatology Project (ISCCP; Rossow and Schiffer 1991) derives cloud amounts and radiative properties from sampled radiances measured by a blend of operational geostationary and polar orbiting satellites. By using the geostationary satellites, ISCCP overcomes the temporal sampling problems which beset climatologies constructed from single polar orbiters, allowing global analyses to be produced for every 3 hours.

Data from Nimbus 7, ERBE and ISCCP have enabled many studies of the Earth's radiation budget and of the distribution and radiative properties of clouds. They have also provided important sources of validation for climate models, as have data from other satellite sensors (including temperature and humidity soundings) and from conventional surface-based measurements and soundings. Unfortunately, with so many different sources for the many geophysical parameters required for climate studies, there is no guarantee of consistency between the various products. Inadequate models for retrieving the required parameters from the

raw data and inadequate sampling in both space and time conspire to add random and systematic errors, which are bound to be different for parameters obtained from different sensors and observing systems.

It is therefore important to know the error characteristics of such datasets and the degree of consistency between them. In the case of the Earth's radiation budget, this should be straightforward. The radiation budget is determined by the distribution of temperature and of the mixing ratios of the radiatively important gases, the distribution and radiative properties of clouds (and to a lesser extent aerosols) and the temperature and radiative properties of the surface. If information is available on all such required input parameters, then it should be possible to simulate the Earth's radiation budget with a suitable radiative transfer scheme and perform comparisons with the satellite data. In practice, there may be considerable practical difficulties in obtaining input data of sufficient accuracy, particularly with regard to clouds. But the differences between the observed and simulated radiation budgets would themselves provide the information required to assess the accuracy both of the input and of the satellite data.

If inconsistencies between the various data sources could be removed, such a simulation system would be a powerful tool for understanding the factors which control the radiation budget. It could be used to fill in locations or periods when satellite data are missing and to provide a means for merging data from satellite experiments performed at different times. The successful simulation of narrow-band data for periods when only these measurements were available would lend credibility to simulations of the broad-band radiation budget for the same periods. In this way, synthetic broad-band information might be extended back in time to the start of the satellite era. Parameters which cannot easily be estimated from satellite data could also be calculated, such as the surface radiation budget and the three dimensional distribution of atmospheric radiative heating, although such products would be particularly sensitive to the input data on clouds and would not be unambiguous (Wu and Chang 1991).

These arguments provided the motivation for the system being developed at the Hadley Centre, known as SAMSON (Simulation and Analysis of Measurements from Satellites using Operational aNalyses). The operational analyses contribute the required atmospheric temperature and humidity fields, and the remaining input data are taken from other sources, as described later. This paper compares SAMSON simulations of the clear-sky Outgoing Longwave Radiation (OLR) over the oceans with ERBE data. In addition, some sensitivity experiments are performed, with particular regard to the optimum temporal resolution of the

simulations.

Similar work has been reported recently by Wu and Susskind (1990), who compared simulations based on geophysical parameters retrieved from satellite infrared and microwave soundings with the Nimbus 7 OLR data, and by Wu and Chang (1991), who examined the sensitivity of their simulations to the substitution of cloud data from ISCCP and other data from various sources. Most of their simulations were performed with temperature and humidity fields derived exclusively from satellite retrievals, whereas SAMSON uses operational analyses. The analyses should provide a better representation of the required fields, because they are produced by combining both satellite remote sensing data and in situ measurements into a physically based model which itself adds information in the form of the background forecast fields and the requirements for dynamical and energy balance.

The present paper concentrates on simulations of the clear-sky OLR over the oceans, as the simplest first test for the system. This is only the first stage in the development of SAMSON, but it will be shown that even this restricted study provides valuable information on the quality both of the analyses and of the ERBE data. Future expansion of SAMSON will include simulations for the whole globe and also for cloudy conditions, allowing some of the applications mentioned earlier to be investigated.

2. Description of SAMSON

SAMSON is constructed as a series of modules, so as to break the simulation problem down into discrete tasks. This allows the maximum of flexibility in choosing the source of the input data and the radiation scheme to be run for a particular application. It also facilitates monitoring of the data as the various tasks are performed. The following sections describe the input data, how these data are interpolated to the simulation grid and the radiation scheme used for the present study.

(a) Input data

Sea surface temperatures were taken from the blended satellite and *in situ* analyses produced by the Climate Analysis Centre at the U.S. National Meteorological Center (Reynolds 1988). The analyses use a flag of -1.8^0 C to denote the presence of sea-ice. For the present study, the SAMSON simulations were performed only over the ice-free oceans, so the flagged points were ignored. The ozone distribution and vertical profile were specified as 5 degree zonal means for each month, based on a climatology for 1979-81 from the Solar Backscatter

Ultraviolet (SBUV) experiment on Nimbus 7 (NASA 1989). Tests show that using ozone data for this period rather than for 1985-86 introduces an error of less than 0.3 Wm^{-2} into the results.

Atmospheric temperatures and humidities were obtained from the archives of two numerical weather prediction centres; the United Kingdom Meteorological Office (UKMO) and the European Centre for Medium-range Weather Forecasts (ECMWF). The use of two distinct sets of analyses allows comparisons which help to identify systematic biases both in the analyses and in the ERBE data. The processing of the analyses was different for the two sources, which will be described in turn.

The UKMO analyses contain temperatures and relative humidities at the pressure levels shown in Table 1. For the period of these simulations, the data are stored as spherical harmonic coefficients at T40 spectral truncation. This study uses only the monthly means, calculated from the daily 0000 GMT and 1200 GMT 'Update' analyses. Surface pressure is not available, but it may be inferred from the geopotential heights of the pressure surfaces, which are stored. Only minor changes were made to the analysis/model system during this period and their impact on the simulations is negligible.

The ECMWF data were obtained from 6-hourly analyses archived at ECMWF. Temperatures and relative humidities (as well as other variables) are stored at the pressure levels shown in Table 1. Surface pressure is also stored. This is essentially the same data source as was used by Hoskins et al. (1989) and contains more levels than the commonly available analyses employed by Wu and Chang (1991; cf. their Table 1). Changes to the model/analysis system are important during this period (as will be demonstrated later) and are summarised in Table 2. The 6-hourly data enable simulations to be made with high temporal resolution. Most of the ECMWF results shown in section 3 were obtained by averaging daily simulations, each of which uses the mean of the four analyses available for that day. For comparison with the UKMO results, simulations were also performed using the monthly mean analyses. The error associated with using such coarse temporal resolution to estimate the monthly mean radiation budget is examined in section 4.

The effect of aerosols on the OLR is not taken into account. The maximum effect is expected from aerosols in the lower stratosphere, because of the large temperature contrast with the surface. It has been estimated that the Mt. Pinatubo eruption in 1991 reduced the OLR by about 1.8Wm^{-2} (Stowe et al. 1992). For the stratospheric aerosol loadings present in 1985 and 1986, the effect is expected to be much smaller and in view of the uncertainties in the other input parameters it is ignored.

(b) Interpolation to the simulation grid

The atmospheric data described above are on fairly coarse vertical grids, especially near to the surface, so the facility was included to interpolate the data to a higher resolution grid before performing the simulations.

For the moisture data, relative humidity is preferred to humidity mixing ratio in performing the vertical interpolation, for two reasons. Firstly, relative humidity varies in the vertical by a much smaller factor than does the mixing ratio. Secondly, interpolating relative humidity ensures that the calculated mixing ratio cannot exceed the saturation value, which might otherwise occur when mixing ratios are interpolated across the tropopause.

The vertical variable for the interpolation is pressure. Temperature, relative humidity and ozone mixing ratios are all interpolated linearly on the logarithm of the pressure. Values close to the surface are obtained by extrapolation from higher levels. Since the UKMO analyses stop at 50mb, the temperatures are extrapolated to obtain values up to the highest input level to the radiation scheme at 10mb (with the constraint that the extrapolated value should not be less than 210K or greater than 240K). For the ECMWF analyses, data were extracted from the archives using the Meteorological Archive and Retrieval System (MARS), at the levels shown in Table 1 and in addition at 950, 70 and 10mb.

As noted in Table 1, the UKMO analyses do not include humidity information above 300mb. A tie-on (Table 3) was therefore constructed, based on the satellite data presented by Jones et al. (1986). Values of the tie-ons at other latitudes are found by linear interpolation of the numbers in the table. The tie-on is expressed in terms of the volume mixing ratio, so the values are converted to relative humidity using the temperatures in the analyses and the composite profile then interpolated onto the simulation grid. The sensitivity of the simulations to the details of the tie-on procedures is small; a $\pm 50\%$ variation of the values in Table 3 changes the simulated OLR by ± 0.9 Wm^{-2} at low latitudes, and by progressively smaller values towards the poles.

The vertical grid for the simulations is based on hybrid coordinates, as is now common in atmospheric general circulation models; it is terrain-following at the lowest levels and isobaric at the highest levels, with a smooth transition inbetween. The pressure p of any level is calculated from a linear combination of a reference pressure p_0 and the surface pressure p_s

$$p = ap_0 + bp_s \qquad (1)$$

where a and b are constants which depend on height. Such a grid allows the number of levels

to be kept constant, whatever the surface pressure, and avoids the numerical problems with terrain-following coordinates in the stratosphere. The number of levels chosen represents a compromise between the competing requirements of minimising the computation time and maximising the resolution to avoid numerical errors in the radiation calculations. It was felt that the resolution of the analyses is too coarse to satisfy the latter requirement, which is clearly crucial. The input data are therefore interpolated to 17 hybrid levels, extending from the surface to 10 mb. Table 4 lists the values of ap_0 and b in (1) for each level and gives examples of the corresponding pressures for two values of the surface pressure. The distribution of the levels changes smoothly both in the vertical and as the surface pressure changes, minimising the risk of numerical problems. The radiation scheme itself adds a further level at about 3×10^{-4} mb (about 100 km altitude) to represent the top of the atmosphere and it assumes that the atmospheric parameters are the same for this level as for the top input level of 10mb. The error associated with using this grid is quantified below. The grid is very similar to that used by many contemporary forecast and climate models and is quite adequate for the present application.

After interpolation, the relative humidity is converted to a mixing ratio and the vertical profiles of temperature, water vapour and ozone mixing ratios, together with the surface pressure and temperature, are passed to the radiation scheme to perform the simulation.

The horizontal grid employed, both for the simulations and for the comparisons with ERBE, is 5 degrees in both latitude and longitude.

(c) Radiation scheme

It is clearly desirable to perform simulations of the radiation budget with as accurate a radiation scheme as possible. The InterComparison of Radiation Codes used in Climate Models (ICRCCM; Ellingson et al. 1991) showed that wide band schemes, which use fewer than about 10 spectral intervals, can be as accurate as narrow band schemes, which may use hundreds of intervals. Unfortunately, a suitable wide band radiation scheme with the required accuracy and including the effects of all the radiatively important gases was not available. For this study, a scheme based on a narrow band Malkmus model was therefore employed (Shine 1991). The scheme was run with a resolution of 10 cm^{-1}, corresponding to 250 spectral intervals from 4μm across the infrared spectrum. The broad-band fluxes were obtained by summing over all the spectral intervals, but in the future it would also be possible to make use of the high spectral resolution of such a scheme to simulate measurements in particular spectral regions. To save computer time, only the fluxes at the top of the atmosphere were calculated.

The accuracy of the scheme as employed in this study was checked by running it in a single column version of SAMSON on the ICRCCM test profiles (Ellingson et al. 1991). In the first test, to determine the accuracy of the radiation scheme itself, the vertical resolution was 1 km, as in the ICRCCM profiles. For the five standard atmospheres with the effects of water vapour, carbon dioxide and ozone included, the average difference between the calculated OLR and that from line-by-line results (Schwarzkopf and Fels 1991, their Table 2) was an underestimate by 0.7 Wm^{-2}, demonstrating excellent agreement with the reference calculations. Unfortunately, this does not provide a measure of the *absolute* accuracy of the Malkmus code, as even the line-by-line models are subject to uncertainties in the spectral line data, the line shape and the water vapour continuum (Ellingson et al. 1991). Radiation code errors have been reduced as much as possible in the present study, but at the present time they cannot be eliminated entirely. In the second test, the comparison was made using the same hybrid grid as in the simulations. The average underestimate of the OLR compared with the line-by-line results increased to 1.8 Wm^{-2}, so the hybrid grid and associated assumptions contribute on average 1.1 Wm^{-2} to the underestimate. This is an acceptable error in view of the fact that uncertainties in the input data, particularly the tropospheric humidities, make the dominant contribution to the overall uncertainty in simulating the OLR, as will be demonstrated.

For the simulations shown below, the effects of the minor and trace constituents nitrous oxide, methane, CFC11 and CFC12 were included, in addition to water vapour, carbon dioxide and ozone. It will be shown in Section 4 that the minor and trace constituents make a significant contribution to the OLR simulations. The volume mixing ratios of the well-mixed gases were prescribed at all points with values appropriate for 1985/6 (IPCC 1990); carbon dioxide 347 x 10^{-6}, nitrous oxide 306 x 10^{-9}, methane 1.69 x 10^{-6}, CFC11 230 x 10^{-12} and CFC12 380 x 10^{-12}. These gases were assumed to have constant mixing ratios both in the horizontal and in the vertical.

3. Simulations of monthly means and comparisons with ERBE

Simulations of the monthly mean clear-sky OLR over the oceans were performed for the period February 1985 to October 1986 (but omitting September 1986); the period for which ERBE comparison data were available. The ERBE fields were obtained from the S-4 archive of merged data from the ERBS and NOAA-9 satellites (Barkstrom et al. 1989). The maps shown focus on the four months selected by the ERBE Science Team for their initial investi-

gations (April, July and October 1985 and January 1986), plus October 1986. In addition, differences between ERBE and the simulations for all the months are shown in a time-latitude plot of the zonal means and as global means.

The ECMWF results shown in the maps are averages of simulations performed for each day of the month, using the diurnal means of the analyses. The UKMO results are single simulations based on the monthly mean analyses. Additional simulations with this reduced temporal sampling were also performed with the ECMWF data. It will be shown later that improving the temporal sampling reduces slightly the differences between ERBE and the ECMWF simulations, and that the differences between the ECMWF and UKMO simulations are dominated by gross differences between the analyses, rather than by details of the temporal sampling employed.

Figure 1 shows the ERBE clear-sky OLR for October 1986 and the simulations made with the ECMWF and UKMO analyses. The simulations reproduce the main features in the ERBE data; not only the broadly zonal nature of the field, but also important departures from zonality such as the local maxima in the sub-tropics and the divergent contour pattern in the N. Atlantic.

Differences between the ERBE data and the simulations for the five months selected for detailed study are shown in Figures 2 and 3. The shaded and hatched areas show differences greater than 5 Wm^{-2} and -5 Wm^{-2}, respectively. Harrison et al. (1990) estimate that the errors in the ERBE monthly mean regional clear-sky OLR are 2 Wm^{-2} for the rms, with a systematic overestimate of about 3-4 Wm^{-2}. The clear areas thus show roughly where the differences are within the errors estimated for the ERBE data. While many details of the differences are due to random errors, there are coherent features which provide valuable information on systematic errors both in the analyses and, to a lesser extent, in the ERBE data. These will be discussed in the following sub-sections.

(a) Changes to the ECMWF model/analysis system

Table 2 lists changes to the ECMWF model/analysis system which were made during this period. The most important changes, as regards the impact on the simulations, are those made in May 1985, although the effect of the March 1986 changes can also be discerned.

In May 1985, several major improvements were made to the ECMWF model. These had a substantial impact both on the analyses and on the forecasts made with the model (Tiedtke et al. 1988). The effect on the clear-sky OLR simulations is apparent in Figure 2. Before implementation of the changes (April 1985), the ERBE clear-sky OLR is higher than

the simulated OLR almost everywhere. In particular, the differences exceed 10 Wm^{-2} through much of the ITCZ. After implementation (July 1985), the simulated OLR increases so that the differences reverse sign and are smaller in magnitude.

The reason for the significant increase in the simulated clear-sky OLR in the tropics is that the changes to the treatment of convection introduced in May 1985 bring about a profound re-distribution of moisture in the analyses (Figure 4). In April 1985, the relative humidity cross section shows a maximum over the equator which extends throughout the troposphere. In July 1985, the boundary layer is deeper and there is a sharp transition to the middle troposphere, which has become much drier. It is the drying of the middle and upper troposphere shown in Figure 4 which increases the simulated clear-sky OLR and produces the reversal in the differences shown in Figure 2. The reduction in the atmospheric moisture content is also apparent in the vertically integrated water vapour mass (often referred to as the 'precipitable' water), the peak values of which are reduced over the ITCZ (Figure 5).

Further reductions in the differences can be seen in Figure 3. By October 1986, the area covered by negative differences is small and the simulations are within 0-5 Wm^{-2} of the ERBE data through much of the tropics.

Figure 6 shows a time-latitude contour plot of the zonal means of the differences between ERBE and the ECMWF simulations, for all the months from February 1985 to August 1986. The domain was restricted to $\pm 60^0$ latitude, to avoid spuriously large differences at high latitudes which result from a few points where ERBE observed sea-ice but the simulations assumed ice-free ocean. The effect of the May 1985 changes can be seen as the reversal in the sign of the differences in the tropics. A less drastic change takes place in March 1986, when the negative region disappears altogether. This is due to the introduction of the revised humidity analysis (Table 2) on 11 March 1986. Animations of the daily simulations show a drop in the clear-sky OLR after this day, as the analyses respond to the change. This is examined further in section 3(c). Another aspect of Figure 6 is that the difference pattern is symmetric about the ITCZ as it moves North-South during the year. For example, in the Northern hemisphere the shaded region is furthest North in August and furthest South in February. Finally, if the suggested ERBE overestimate of 3-4 Wm^{-2} was subtracted from the figure, then at the end of the period studied it would show small negative values in the tropics (consistent with the analyses being too dry) and small positive values in the sub-tropics and middle latitudes (consistent with the analyses being too moist). The presence of such residual errors in the analyses is consistent with the conclusions of Liu et al. (1992), based on comparisons of ECMWF analyses for 1987-

88 with retrievals of precipitable water from the Special Sensor Microwave/Imager (SSM/I).

(b) Differences between the ECMWF and UKMO analyses

Many of the differences between the clear-sky OLR simulations using the ECMWF and UKMO analyses are attributable to differences between the moisture distributions in the analyses. For example, in April 1985 there is a good correspondence at low latitudes between negative OLR differences (Figure 7, top left) and positive differences greater than 5 kgm^{-2} in the vertically integrated water vapour density (Figure 7, top right). The fact that smaller positive differences in the latter field are associated with positive OLR differences (for example in much of the southern hemisphere), contrary to the expectation that a moister profile should reduce the OLR, indicates that other factors are also operating, such as differences in the distribution of the moisture in the vertical.

After the changes to the ECMWF model discussed above, the pattern in the clear-sky OLR differences is altered radically. In July 1985, there are now positive maxima throughout the tropics (Figure 7, lower left). However, the differences between the vertically integrated water vapour density (Figure 7, lower right) show only modest changes compared with April 1985. This shows that the drying of the ECMWF analyses in the middle and upper troposphere is the controlling factor which increases the simulated clear-sky OLR. Even so, it is still true that the largest positive differences in the vertically integrated water vapour densities (Figure 7, lower right) are associated with *relative* minima in the OLR differences.

These plots demonstrate that differences between the simulated clear-sky OLR from the two sets of analyses can be produced by differences both in the vertical distribution of moisture and in its vertical integral. The changes to the moisture distribution in the ECMWF model can be understood in terms of the small number of relevant changes which were made to the model in May 1985, as noted in the previous sub-section. However, it is much more difficult to explain the differences between two sets of analyses, because of the much larger number of differences between the two model and analysis systems. Such explanations are beyond the scope of this paper and will not be attempted. Nevertheless, it is valuable to determine whether the differences between the analyses exceed the errors attributed to elements of the observing system which provide the required input. Radiosonde comparisons show that measurements of temperature can be made to an accuracy of better than about ±1 K and of relative humidity to about ±10% (Nash and Schmidlin 1987). Applying systematic perturbations of these amounts to the analyses produces changes in the simulated OLR of up to ± 1.5 Wm^{-2} for temperature and up to ± 3 Wm^{-2} for relative humidity. Differences between the anal-

yses are indeed of order 1 K for temperature but can be several tens of percent for relative humidity. This indicates that the analyses are generally consistent in their representation of the temperature field and that temperature is not a serious source of error in the simulations. In contrast, relative humidity differences between the analyses are larger than the errors attributed to radiosondes and explain the differences between the simulations shown in Figure 7. The large change in the ECMWF simulations following May 1985 confirms that the formulation of a model strongly influences the analyzed relative humidity field. This is inevitable over the oceans in view of the sparsity of radiosonde data and the reliance on the model in these regions. It confirms the importance of making the best use of satellite data to help improve the humidity analyses (Illari 1989).

(c) Global means and differences

Global means of the ERBE data and of the simulations for February 1985 to August 1986 are shown in the upper panel of Figure 8. The lower panel shows the differences between ERBE and the simulations. The means and differences are for the oceans only and, as in Figure 6, are restricted to latitudes less than $\pm 60^0$ to avoid points where ERBE observed sea-ice but the simulations assumed ice-free ocean. Each data point was weighted by the cosine of the latitude to correct for the latitude-longitude grid.

The ERBE means are higher than those from the simulations and show significant month to month variability, with an amplitude of about 4 Wm^{-2}. This is over twice the amplitude in the UKMO simulations. The ECMWF daily simulations show the effects of the two major changes to the model/analysis system in May 1985 and March 1986. In each case, the global means change by about 3 Wm^{-2}, although in opposite directions.

The ECMWF differences compared with ERBE are shown both for the averages of the daily simulations (as shown in Figures 2 and 3) and for the single simulations performed with the monthly mean analyses (as for the UKMO results). The differences for the monthly simulations are about 0.6 Wm^{-2} higher than for the daily simulations, reflecting the small systematic error introduced by the poorer temporal sampling (see section 4(c)). Prior to the introduction of the changes to the ECMWF model in May 1985, all the simulations are on average about 8 Wm^{-2} lower than the ERBE values. After that time, the ERBE-ECMWF differences drop sharply and then average about 4 Wm^{-2}, while the ERBE-UKMO differences average about 7 Wm^{-2}. There is considerable scatter in the differences, which the top panel shows is mainly due to the scatter in the ERBE means. For example, from April to June 1985 there are drops in the ERBE means, which amplify the effect of the May 1985 changes to the ECMWF model and

are also reflected in the ERBE-UKMO differences. In addition, a further drop in the ERBE means takes place at about the same time as the March 1986 changes to the ECMWF model. This reduces the impact of the changes on the ERBE-ECMWF differences and also accounts for the weak signal in the time-latitude plot at this time (Figure 6).

If the ERBE overestimate of 3-4 Wm^{-2} is subtracted from these differences, then Figure 8 suggests that the ECMWF global means at the end of the period are close to the real values and that the UKMO global means are 2-3 Wm^{-2} too low. There are of course significant geographical variations in the differences and several uncertainties both in the input data and in the radiation modelling which are of order 1 Wm^{-2}, as noted earlier. It could therefore be coincidental that the ERBE systematic error and the ERBE-ECMWF differences have the same value.

4. Sensitivity tests

(a) Minor and trace constituents

Many general circulation models used for numerical weather prediction and climate research do not include the effects of certain minor and trace constituents (nitrous oxide, methane, CFC11 and CFC12) on the longwave fluxes, although efforts to include them in a computationally efficient manner have been made (e.g. Wang et al. 1991). The importance of these gases to a proper calculation of the clear-sky OLR is illustrated in Figure 9, which shows the difference between the April 1985 simulation with the monthly mean ECMWF analysis and the same calculation omitting these gases. The difference is over 5 Wm^{-2} at low latitudes, decreasing to below 4 Wm^{-2} at high latitudes. The largest differences are not on the equator but in the sub-tropics, where the moisture contents are much lower (cf. Figure 5), reducing the masking effect from overlapping water vapour absorption. The magnitude of the differences is comparable with the differences shown in Figure 8, illustrating the importance of accounting for the minor and trace constituents in these simulations.

(b) Diurnal sampling of the analyses

The simulations discussed in the previous sections use all the available analyses for a given month, so that the diurnal cycle is covered in the ECMWF simulations by averaging the 0000, 0600, 1200 and 1800 GMT analyses. The importance of adequate diurnal sampling was investigated by repeating the April 1985 simulation with the monthly mean analysis four times, using the data from each of the four synoptic hours separately. Figure 10 shows the differences between each of these simulations and the simulation which uses all the available analyses.

Each frame thus shows the systematic error which results from performing the simulation with data from only one of the synoptic hours. There is a clear wavenumber 1 pattern in the differences, which propagates westwards with a period of one day. This is despite the fact that the simulations are performed only over the oceans and the sea surface temperature data have no diurnal cycle. The result is thus due to diurnal variations in the atmospheric analyses. The peak-to-peak amplitude of the pattern is only about 2 Wm^{-2}, so that even if, for example, only the 0000 GMT data were averaged to create the monthly mean, the systematic error introduced would be small. A much larger error would be expected for simulations performed over land, for which it is probably necessary to perform a sufficient number of simulations to resolve the diurnal cycle explicitly.

(c) Temporal sampling of the monthly analyses

A problem which is related to diurnal sampling arises from the non-linear response of the OLR to changes in the atmospheric temperatures and humidities. Synoptic or low frequency variability of these parameters should ensure that a single simulation using the monthly mean analysis gives different answers from the mean of a set of simulations using analyses averaged over a shorter timescale which resolves the variability. The latter approach is closer to the real world, but requires more simulations and so is computationally more expensive.

The magnitude of this effect may be found by comparing the ECMWF simulations which use the monthly mean analyses with the means of the simulations performed for each day. The comparison of the global averages in Figure 8 shows that the daily simulations are indeed superior, in so far as they reduce slightly the differences compared with ERBE. A more detailed investigation was carried out for January 1986, using additional simulations for which the daily mean analyses were averaged over progressively longer periods and simulations then made to produce different realisations of the monthly mean clear-sky OLR. The additional averaging periods were 3, 5 and 10 days. Since none of the additional periods divide equally into 31, one of the simulations in each case had to include one additional day and the individual simulations were then weighted accordingly.

Figure 11 shows the differences between the means of the simulations performed using analyses averaged over 3, 5, 10 and 31 days (only one simulation in this case) and the benchmark monthly mean obtained by averaging the 31 daily simulations. With 3-day averaging, there is negligible error in simulating the monthly mean clear-sky OLR. As the averaging period increases from 3 to 10 days, the error gradually increases and becomes negative almost everywhere (which is to be expected from the form of the non-linear dependence of the OLR

on changes in both temperature and humidity), although even with 10 day averaging the maximum error is only 2 Wm^{-2}. When the monthly mean analysis is used, an isolated maximum appears at 115^0W, which is discussed in the following paragraph. Elsewhere, there is a further modest increase in the error compared with the other plots, with the maxima concentrated in the sub-tropics. These maxima are just visible with 5-day averaging and grow steadily thereafter, indicating that they are due to the mis-representation of low-frequency variability on timescales between about 5 days and one month. This is consistent with Duvel (1988), who showed that most of the variance in the METEOSAT window and water vapour channel radiances over the sub-tropics is concentrated on timescales longer than about 9 days.

The maximum at 115^0W for the simulation with the monthly mean analysis shows a different behaviour from the other sub-tropical maxima. There is only a weak feature in the 10-day error map, displaced to the West, suggesting that the timescale of the variability which gives rise to the error is longer than 10 days. Inspection of the individual simulations and analyses shows that the maximum is caused by extremely low relative humidities over this region in the middle and upper troposphere during the first ten days of the month, followed by a gradual recovery to more typical values later in the month (Figure 12). The low relative humidities appear at the same time as strong north-south cross-equatorial flow at 200mb (ECMWF 1987). The humidity minimum leads to a simulated clear-sky OLR which at the beginning of the month exceeds 310 Wm^{-2} over this feature, but the ERBE data averaged over the same period show no evidence for such an extreme maximum (Figure 13). This suggests that the behaviour of the ECMWF humidities in this region is unphysical and is caused by a problem in the analyses. The fact that this problem was uncovered by performing these simulations demonstrates a further application for SAMSON in helping to assess the physical realism of the humidity analyses.

Examination of such difference maps for other months confirms the results shown in Figure 11, although the isolated maximum at 115^0W in this month is twice the magnitude and more extensive than similar features in other months. If this maximum is taken to be due to an isolated problem with the humidities in the ECMWF analyses, then Figure 11 suggests that the error associated with estimating the monthly mean clear-sky OLR from a single simulation using the monthly mean analysis is at most about -2 Wm^{-2} and Figure 8 shows that the global mean (over the oceans) is underestimated by about 0.6 Wm^{-2}. In the storm tracks the error is less than -1 Wm^{-2}, despite the fact that these areas are known to show considerable synoptic variability. It is possible that much of this variability has been removed by the 5 degree spatial

and one day temporal resolution used to perform the 'benchmark' simulation. It would thus be valuable to check the validity of these results by performing simulations at higher spatial and temporal resolution. Finally, it should be noted that the monthly mean radiation budget is employed in this study primarily to allow comparisons with ERBE. The calendar month provides a convenient averaging period, but it is not necessarily the best for studying the radiation budget, given the significant intra-seasonal variability at low latitudes.

5. Discussion

It has been shown that it is possible to simulate the clear-sky OLR over the oceans, using operational analyses and other information, with an accuracy comparable with that of the ERBE product. The systematic differences between the ERBE data and the simulations provide valuable information on the quality of the analyses and in particular on systematic errors in the humidities. Following the changes to the ECMWF model in May 1985, the global averages of the differences between the ECMWF simulations and the ERBE data are consistent with the known ERBE overestimate of 3-4 Wm^{-2}. The global differences for the UKMO simulations are slightly larger.

In making such comparisons it is important to remember the many differences between the strategies employed by ERBE and SAMSON to obtain the clear-sky flux, apart from the obvious difference between observation and simulation. ERBE uses a scene identification algorithm to determine when a scanner pixel is cloud-free (Wielicki and Green 1989). Unusually moist (but cloud-free) profiles which produce a lower than expected OLR may be classified incorrectly as cloudy, producing a systematic positive bias in the archived clear-sky OLR. In addition, for obvious reasons ERBE obtains a clear-sky flux only when the algorithm deems a pixel to be cloud-free. The clear-sky flux is thus found by Method I of Cess and Potter (1987); the clear-sky fluxes come only from the cloud-free pixels. In contrast, SAMSON calculates the clear-sky OLR at each grid point, regardless of the cloud cover, so there are no missing data points as are present in the ERBE data. This is Cess and Potter's Method II, which is consistent with the concept of cloud radiative forcing as applied to general circulation and climate models (Potter et al. 1992). As with the models, the operational analyses used by SAMSON represent averages over a grid box and are thus not biased to either cloudy or cloud-free regions. However, differences between the atmospheric temperatures and humidities in these regions could produce corresponding differences between the Method I and II estimates of the clear-sky

OLR. For example, if humidities are lower in the cloud-free regions, as might be expected, this would contribute to the positive bias in the ERBE values. The magnitude of the Method I/II bias could be confirmed by simulation studies, but to be conclusive they would need to be performed at the same spatial and temporal resolution as that employed by ERBE. Such a comprehensive study has not yet been performed, although a valuable step in this direction has been taken by Potter et al. (1992).

Even small systematic biases in the clear-sky OLR may still be important. For example, a 3 Wm^{-2} overestimate of the global average clear-sky flux translates into a 10% overestimate of the derived cloud longwave radiative forcing, which is the relatively small difference between the total and clear-sky fluxes. If the cloud forcing is required to higher accuracy this places considerable demands on the accuracy of the clear-sky flux.

The use of operational numerical weather prediction analyses to provide the required atmospheric temperature and humidity fields is an important aspect of SAMSON. As noted in the introduction, these analyses should constitute the best available description of these fields. However, the comparisons between the simulations using the ECMWF and UKMO analyses show a significant sensitivity to the humidity fields, which probably represent the largest source of error in the simulations. There is evidence that the changes to the ECMWF model/analysis system during 1985/6 have improved the humidity analyses. This will be investigated further by performing simulations and comparisons with ERBE for the period beyond the end of 1986, and by including independent information on the vertical integral of the water vapour densities retrieved from microwave radiometer data.

These results also provide support for proposals to re-analyse past data for as far back in time as possible, using the best available model/analysis system which remains fixed for the period of the re-analysis (Bengtsson and Shukla 1988). The latter requirement is essential in order to remove the steps introduced by analysis changes, the effect of which is graphically illustrated in Figure 8. For the radiation budget calculations, the most important requirement would be the improvement of the humidity analyses, which would hopefully allow the errors in the simulated clear-sky fluxes to be reduced further. Simulations with such improved analyses could be performed by SAMSON, but they could also be performed within the model as the re-analysis proceeds, so that the full temporal, horizontal and vertical resolution of the model could be utilised. Such calculations could then provide a reference for subsequent simulations and for comparisons with satellite data.

If simulations of at least the clear-sky component of the radiation budget can be per-

formed with an accuracy comparable with or better than that achieved by ERBE, there are implications for planning future satellite experiments. The temporal and spatial sampling provided by the analyses cannot be matched by a space-based system unless several satellites are employed. In addition, a significant portion of the complexity of the ERBE instrumentation and data analysis system stems from the requirement to estimate the clear-sky fluxes. If this requirement could be relaxed by developing a hybrid system in which some or even all of the clear-sky fluxes were obtained by simulation rather than by observation, this might lead to significant savings. The satellite component of such a system could then focus on the measurement of the total fluxes. For this approach to succeed, it would be necessary to ensure that the input parameters not covered by operational analyses (such as the concentrations of ozone, minor and trace constituents and perhaps aerosols) were obtained with the necessary accuracy.

The results and comparisons shown in this paper have demonstrated the power of the SAMSON system, albeit for the restricted case of the clear-sky outgoing OLR over the oceans. The system is currently being expanded to simulate not only the clear-sky but also the total fluxes over both land and sea, by including cloud and additional data from ISCCP. Comparisons with ERBE will remain a most important part of this work.

Acknowledgements

The Malkmus narrow band radiation code was generously provided by Dr. K.P. Shine of the University of Reading. The figures were produced with the PCMDI Graphics package, developed and made available by staff of the Program for Climate Model Diagnosis and Intercomparison at the Lawrence Livermore National Laboratory. The ERBE data were obtained from the World Data Centre A, at the Goddard Space Flight Center. Valuable comments on the manuscript were received from J.R. Eyre, E.F. Harrison, P. Minnis, K.P. Shine and A. Simmons. This work was funded by the U.K. Department of the Environment under contract PECD 7/12/37.

References

Ardanuy, P.E., Stowe, L.L., Gruber, A., Weiss, M. and Long, C.S., 1989. Longwave cloud radiative forcing as determined from Nimbus-7 observations. *J. Clim.*, **2**, 766-799

Barkstrom, B.R., 1984. The Earth Radiation Budget Experiment (ERBE). *Bull. Amer. Meteorol. Soc.*, **65**, 1170-1185

Barkstrom, B., Harrison, E., Smith, G., Green, R., Kibler, J., Cess, R. and the ERBE Science Team, 1989. Earth Radiation Budget Experiment (ERBE) archival and April 1985 results. *Bull. Amer. Meteorol. Soc.*, **70,** 1254-1262

Bengtsson, L. and Shukla, J., 1988. Integration of space and in situ observations to study global climate change. *Bull. Amer. Meteorol. Soc.*, **69,** 1130-1143

Cess, R.D. and Potter, G.L., 1987. Exploratory studies of cloud radiative forcing with a general circulation model. *Tellus*, **39A,** 460-473

Duvel, J.P., 1988. Analysis of diurnal, interdiurnal and interannual variations during northern hemisphere summers using METEOSAT infrared channels. *J. Clim.*, **1,** 471-484

ECMWF, 1987. *Daily Global Analyses, January - March 1986*. European Centre for Medium Range Weather Forecasts, Shinfield Park, Reading RG2 9AX, England.

Ellingson, R.G., Ellis, J. and Fels, S., 1991. The intercomparison of radiation codes used in climate models: Long wave results. *J. Geophys. Res.*, **96,** 8929-8953

Harrison, E.F., Minnis, P., Barkstrom, B.R., Ramanathan, V., Cess, R.D. and Gibson, G.G., 1990. Seasonal variation of cloud radiative forcing derived from the Earth Radiation Budget Experiment. *J. Geophys. Res.*, **95,** 18687-18703

Hoskins, B.J., Hsu, H.H., James, I.N., Masutani, M., Sardeshmukh, P.D. and White, G.H., 1989. *Diagnostics of the global atmospheric circulation based on ECMWF analyses 1979-1989*. WCRP-27 (WMO/TD - No. 326), World Meteorological Organization

Illari, L., 1989. The quality of satellite precipitable water content data and their impact on analyzed moisture fields. *Tellus*, **41A,** 319-337

IPCC, 1990. *Climate Change. The IPCC Scientific Assessment*. Eds. J.T. Houghton, G.J. Jenkins and J.J. Ephraums. Cambridge University Press

Jones, R.L., Pyle, J.A., Harries, J.E., Zavody, A.M., Russell, J.M. and Gille, J.C., 1986. The water vapour budget of the stratosphere studied using LIMS and SAMS satellite data. *Q. J. R. Meteorol. Soc.*, **112,** 1127-1143

Kyle, H.L., Ardanuy, P.E. and Hurley, E.J., 1985. The status of the Nimbus 7 Earth Radiation Budget data set. *Bull. Amer. Meteorol. Soc.*, **66,** 1378-1388

Liu, W.T., Tang, W. and Wentz, F.J., 1992. Precipitable water and surface humidity over global oceans from special sensor microwave imager and European Center for Medium range Weather Forecasts. *J. Geophys. Res.*, **97,** 2251-2264

NASA, 1989. *Nimbus-7 Data Product Summary*. NASA Reference Publication 1215. National Aeronautics and Space Administration, Washington, D.C. 20546, U.S.A.

Nash, J. and Schmidlin, F.J., 1987. *WMO International Radiosonde Comparison (U.K. 1984, U.S.A. 1985). Final Report.* Instruments and Observing Methods Report No. 30, WMO/TD-No. 195, World Meteorological Organization, Geneva

Potter, G.L., Slingo, J.M., Morcrette, J.-J. and Corsetti, L., 1992. A modeling perspective on cloud radiative forcing. *J. Geophys. Res.*, in press

Ramanathan, V., Cess, R.D., Harrison, E.F., Minnis, P., Barkstrom, B.R., Ahmad, E. and Hartmann, D., 1989. Cloud-radiative forcing and climate: Results from the Earth Radiation Budget Experiment. *Science*, **243,** 57-63

Reynolds, R.W., 1988. A real-time global sea surface temperature analysis. *J. Climate*, **1,** 75-86

Rossow, W.B. and Schiffer, R.A., 1991. ISCCP cloud data products. *Bull. Amer. Meteorol. Soc.*, **72,** 2-20

Schwarzkopf, M.D. and Fels, S.B., 1991. The simplified exchange method revisited: An accurate, rapid method for computation of infrared cooling rates and fluxes. *J. Geophys. Res.*, **96,** 9075-9096

Shine, K.P., 1991. On the cause of the relative greenhouse strength of gases such as the halocarbons. *J. Atmos. Sci.*, **48,** 1513-1518

Stephens, G.L. and Greenwald, T.J., 1991. The Earth's radiation budget and its relation to atmospheric hydrology: 2. Observations of cloud effects. *J. Geophys Res.*, **96,** 15325-15340

Stowe, L.L., Yeh, H.Y.M., Eck, T.F., Wellemeyer, C.G., Kyle, H.L. and the Nimbus-7 Cloud Data Processing Team, 1989. Nimbus-7 global cloud climatology. Part II: First year results. *J. Clim.*, **2,** 671-709

Stowe, L.L., Carey, R.M. and Pellegrino, P.P., 1992. Monitoring the Mt. Pinatubo aerosol layer with NOAA/11 AVHRR data. *Geophys. Res. Letts.*, **19,** 159-162

Tiedtke, M., Heckley, W.A. and Slingo, J., 1988. Tropical forecasting at ECMWF: The influence of physical parametrization on the mean structure of forecasts and analyses. *Q. J. R. Meteorol. Soc.*, **114,** 639-664

Wang, W.-C., Shi, G.-Y. and Kiehl, J.T., 1991. Incorporation of the thermal radiative effect of CH_4, N_2O, CF_2Cl_2, and $CFCl_3$ into the National Center for Atmospheric Research Community Climate Model. *J. Geophys. Res.*, **96,** 9097-9103

Wielicki, B.A. and Green, R.N., 1989. Cloud identification for ERBE radiative flux retrieval. *J. Appl. Meteorol.*, **28,** 1133-1146

Wu, M.-L. C. and Chang, L.A., 1991. Differences in global data sets of atmospheric and surface parameters and their impact on outgoing longwave radiation and surface downward flux calculations. *J. Geophys. Res.*, **96,** 9227-9262

Wu, M.-L. C. and Susskind, J., 1990. Outgoing long-wave radiation computed from HIRS2/MSU soundings. *J. Geophys. Res.*, **95,** 7579-7602

TABLE 1. Pressure levels in the UKMO and ECMWF archived operational analyses

UKMO	ECMWF
	30
50*	50
70*	-
100*	100
150*	150
200*	200
250*	250
300	300
400	400
500	500
700	700
850	850
1000	1000

* Humidity information is not available at these levels. See section 2(b)

TABLE 2. Important changes to the ECMWF model/analysis system for the period covering the simulations (Source: Hoskins et al. 1989).

Date	Brief details of change
May 1985	T106 model with reduced horizontal diffusion, shallow convection, modified Kuo scheme and new representation of cloudiness
Oct. 1985	Analysis uses 11 instead of 14 layers of satellite data
Dec. 1985	Modified subterranean extrapolation
March 1986	Tides handled by initialization
March 1986	Improved humidity analysis, including use of satellite precipitable water content data
May 1986	Three new levels in stratosphere
July 1986	Gravity wave drag parametrization
Sept. 1986	New analysis, including analysis at model levels and further refined structure functions

TABLE 3. Humidity mixing ratios tied on to the UKMO analyses

	Volume mixing ratio (x 10^{-6})		
Pressure (mb)	90^0 N	Equator	90^0 S
10	5	5	5
70	5	2.5	5
150	5	8	5

TABLE 4. Values of the constants ap_0 and b for the hybrid levels used to input data to the radiation scheme, and of the corresponding pressures for two different values of the surface pressure p_s. All pressures are in millibars. A further level at about 3×10^{-4} mb is added by the radiation scheme to account for the atmosphere above 10 mb (see text).

Hybrid constants		Pressure levels	
ap_0	b	p_s=1000	p_s=700
10	0	10	10
30	0	30	30
50	0	50	50
70	0	70	70
100	0	100	100
150	0	150	150
196.875	0.028125	225	216.6
225	0.075	300	277.5
250	0.15	400	355.0
250	0.25	500	425.0
225	0.375	600	487.5
175	0.525	700	542.5
96.875	0.678125	775	571.6
0	0.85	850	595.0
0	0.9	900	630.0
0	0.95	950	665.0
0	1	1000	700

Figure captions

Figure 1. Monthly mean clear-sky Outgoing Longwave Radiation (OLR) over the oceans for October 1986 from ERBE and from the simulations using the ECMWF and UKMO analyses. The ECMWF simulations were performed for each day of the month, using the diurnal means of the analyses, and then averaged. The UKMO simulation used only the monthly mean analysis. The contour interval is 10 Wm^{-2} and values above 290 Wm^{-2} are shaded.

Figure 2. Differences between the ERBE monthly mean clear-sky Outgoing Longwave Radiation (OLR) over the oceans and the simulations with the ECMWF and UKMO analyses, for April and July 1985. The ECMWF simulations were performed for each day of the month, using the diurnal means of the analyses, and then averaged. The UKMO simulations used only the monthly mean analysis. The contour interval is 5 Wm^{-2}. Differences greater than 5 Wm^{-2} are shaded and differences greater than -5 Wm^{-2} are hatched.

Figure 2. Continued.

Figure 3. Same as Figure 2, but for October 1985, January 1986 and October 1986.

Figure 3. Continued.

Figure 4. Cross sections of the zonally averaged relative humidity from the ECMWF monthly mean analyses, for April and July 1985. The contour interval is 5 per cent and the pressure in mb is shown on the left.

Figure 5. Vertically integrated water vapour density from the ECMWF monthly mean analyses, for April and July 1985. The contour interval is 5 kgm^{-2} and values above 30 kgm^{-2} are shaded.

Figure 6. Time-latitude plot of the zonally averaged differences between the ERBE monthly mean clear-sky Outgoing Longwave Radiation (OLR) over the oceans and the monthly mean of the daily simulations with the ECMWF analyses, for February 1985 to August 1986. The contour interval is 5 Wm^{-2}. Differences greater than 5 Wm^{-2} are shaded and differences greater

than -5 Wm^{-2} are hatched. Values poleward of $\pm 60^0$ latitude are not shown, as there are spuriously large differences caused by a few points where ERBE observed sea-ice but the simulations assumed ice-free ocean.

Figure 7. Differences between the simulated clear-sky Outgoing Longwave Radiation (OLR) over the oceans using the ECMWF daily and the UKMO monthly mean analyses (left) and between the vertically integrated water vapour densities from the same analyses (right), for April and July 1985. The contour interval for the OLR differences is 5 Wm^{-2} and for the vertically integrated water vapour density differences is 5 kgm^{-2}. In both cases, differences greater than 5 units are shaded and differences greater than -5 units are hatched.

Figure 7. Continued.

Figure 8. Global means of the ERBE and simulated clear-sky Outgoing Longwave Radiation (OLR) over the oceans (upper panel) and differences between the ERBE and simulated global means (lower panel), for February 1985 to August 1986. The domain is restricted to $\pm 60^0$ latitude, to avoid points where ERBE observed sea-ice but the simulations assumed ice-free ocean.

Figure 9. Difference between the April 1985 simulated clear-sky Outgoing Longwave Radiation (OLR) over the oceans using the ECMWF monthly mean analysis, but omitting the minor and trace constituents (nitrous oxide, methane, CFC11 and CFC12), and the normal simulation which includes these gases. The contour interval is 0.5 Wm^{-2} and differences greater than 5 Wm^{-2} are shaded.

Figure 10. Differences between the April 1985 simulated clear-sky Outgoing Longwave Radiation (OLR) over the oceans using the ECMWF analyses for only 0000, 0600, 1200 and 1800 GMT and the simulation using the monthly mean analysis. The contour interval is 1 Wm^{-2} and negative values are shaded.

Figure 11. Differences between the January 1986 simulated clear-sky Outgoing Longwave Radiation (OLR) over the oceans using the ECMWF analyses, obtained from simulations performed with analyses averaged over periods of 3, 5, 10 and 31 days, and a benchmark averaged

from 31 simulations performed with the daily mean analyses. The contour interval is 1 Wm^{-2} and positive values are shaded.

Figure 11. Continued.

Figure 12. North-South vertical cross sections at longitude $115^{0}W$ through the relative humidities from the January 1986 ECMWF analyses, averaged over the first 5 days of the month (top) and the last 5 days (bottom). The contour interval is 5 per cent and the pressure in mb is shown on the left.

Figure 13. Comparison of the simulated clear-sky Outgoing Longwave Radiation (OLR) over the oceans using the ECMWF analyses averaged over the first 5 days of January 1986 (top) and the ERBE data for the same period (bottom). The contour interval is 10 Wm^{-2} and values above 290 Wm^{-2} are shaded.

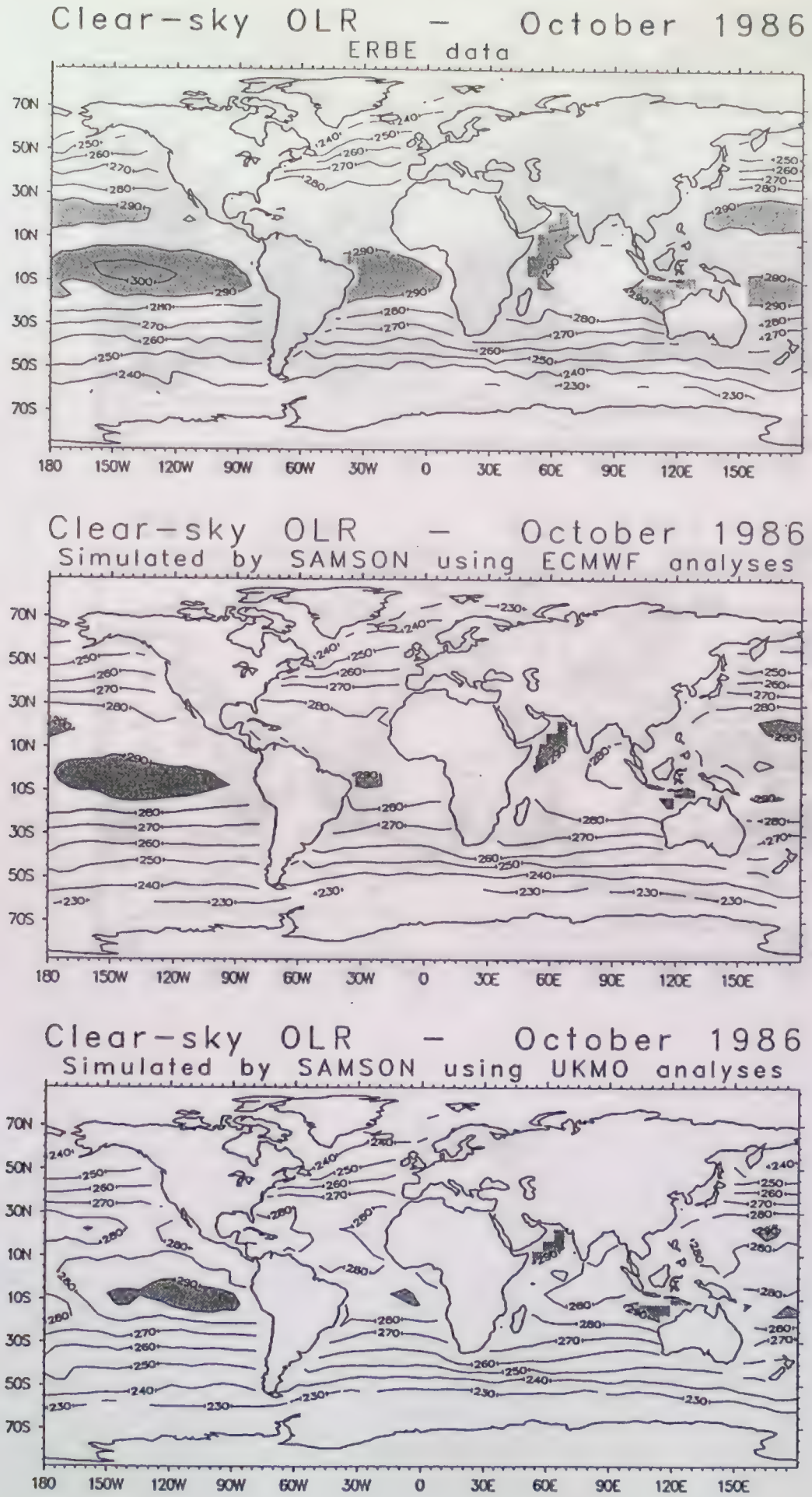
Clear-sky OLR - October 1986
ERBE data
Clear-sky OLR - October 1986
Simulated by SAMSON using ECMWF analyses
Clear-sky OLR - October 1986
Simulated by SAMSON using UKMO analyses
70N
50N
30N
10N
10S
30S
50S
70S
180
150W
120W
90W
60W
30W
0
30E
60E
90E
120E
150E

Figure 1

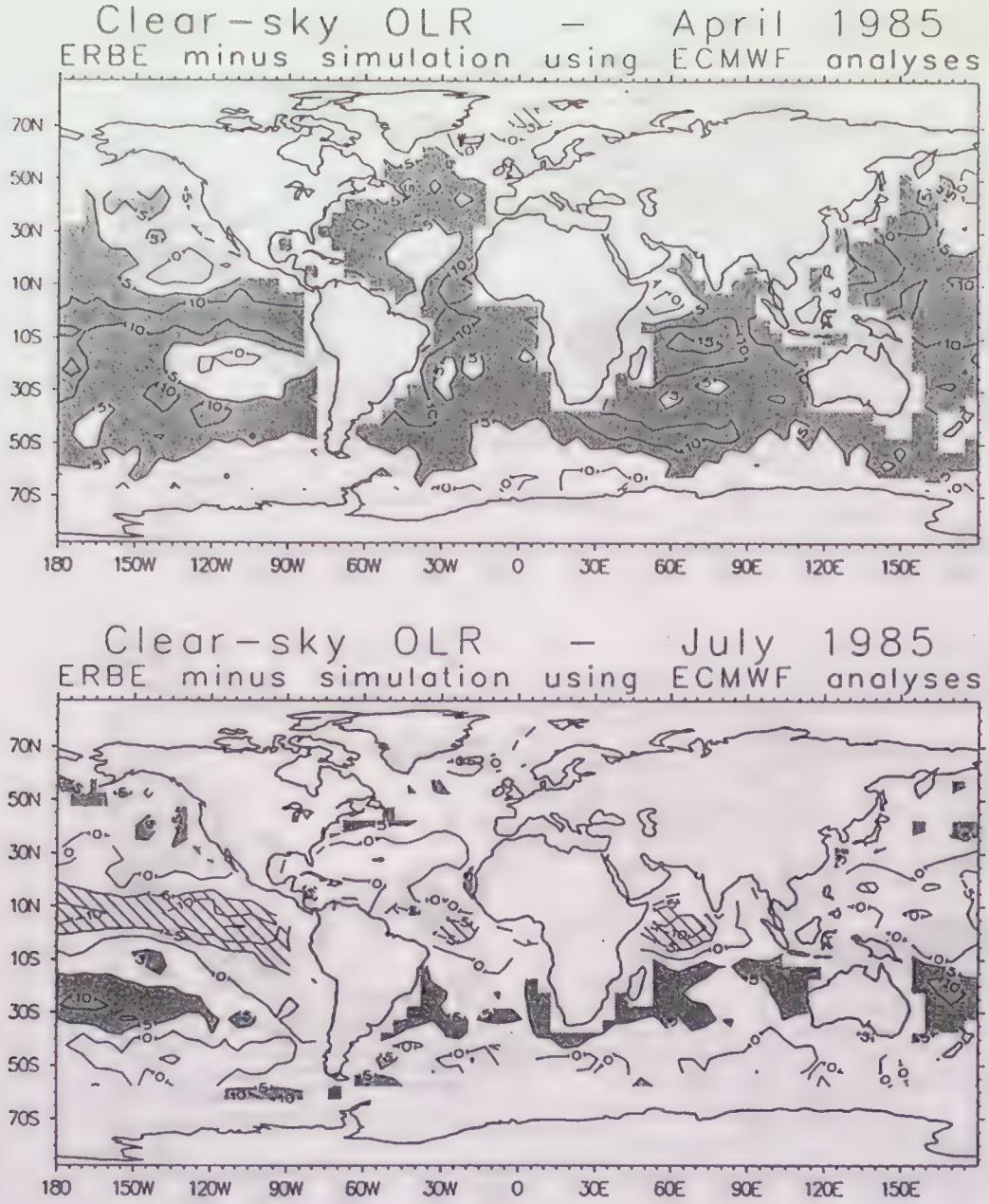
Clear-sky OLR – April 1985
ERBE minus simulation using ECMWF analyses
70N
50N
30N
10N
10S
30S
50S
70S
180
150W
120W
90W
60W
30W
0
30E
60E
90E
120E
150E
Clear-sky OLR – July 1985
ERBE minus simulation using ECMWF analyses
70N
50N
30N
10N
10S
30S
50S
70S
180
150W
120W
90W
60W
30W
0
30E
60E
90E
120E
150E

Figure 2

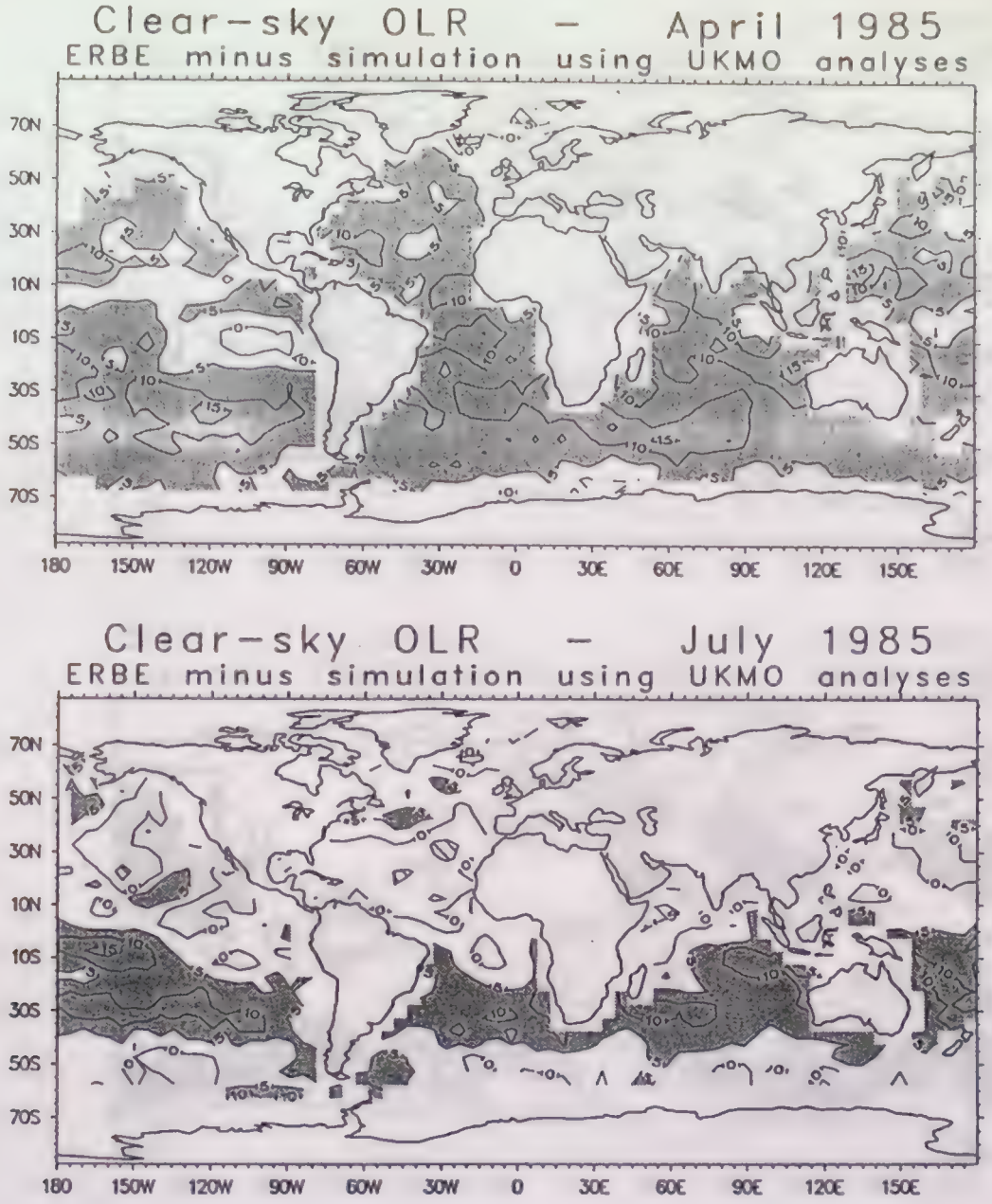

Figure 2 (continued)

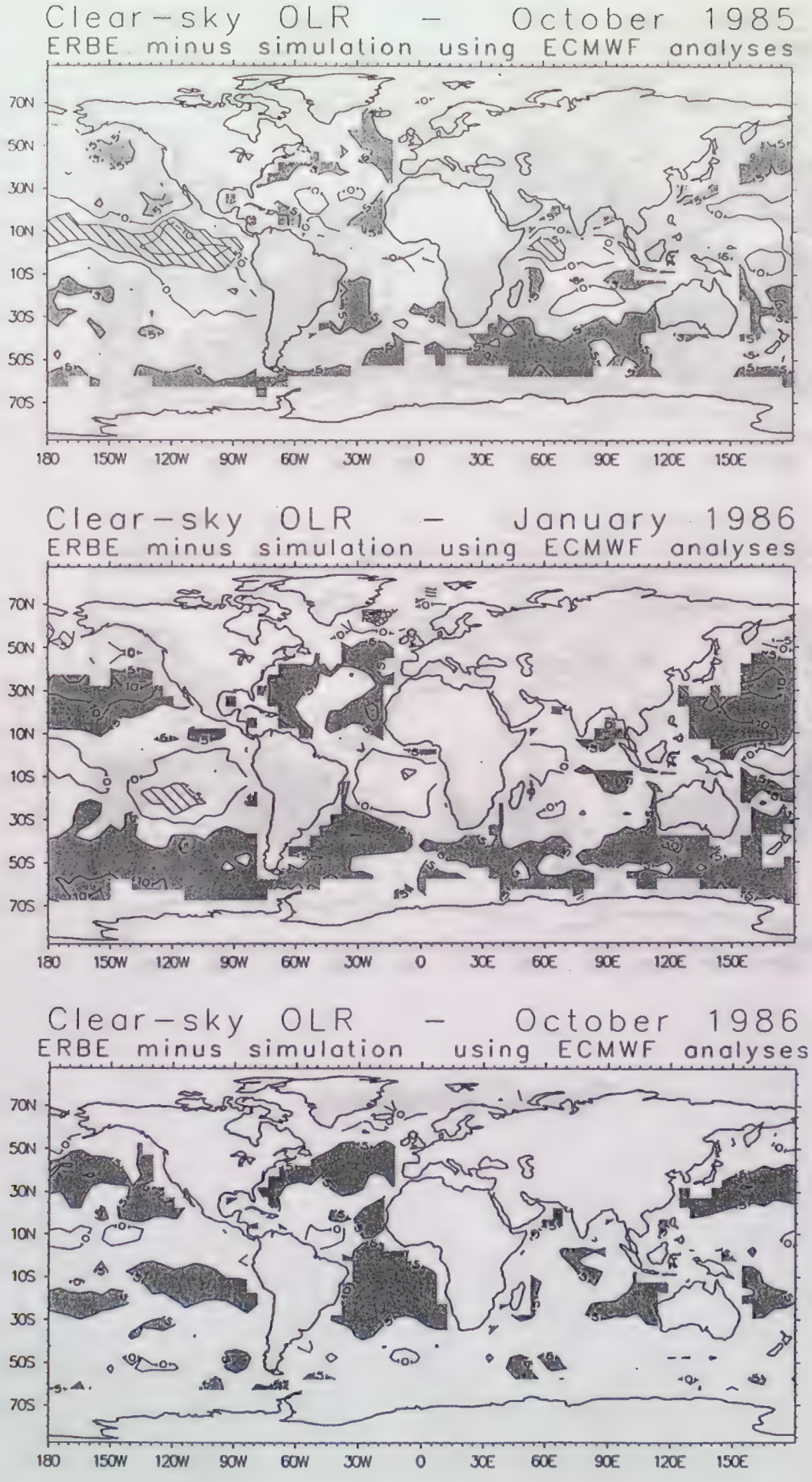
Clear-sky OLR - October 1985
ERBE minus simulation using ECMWF analyses
Clear-sky OLR - January 1986
ERBE minus simulation using ECMWF analyses
Clear-sky OLR - October 1986
ERBE minus simulation using ECMWF analyses
70N
50N
30N
10N
10S
30S
50S
70S
180 150W 120W 90W 60W 30W 0 30E 60E 90E 120E 150E

Figure 3

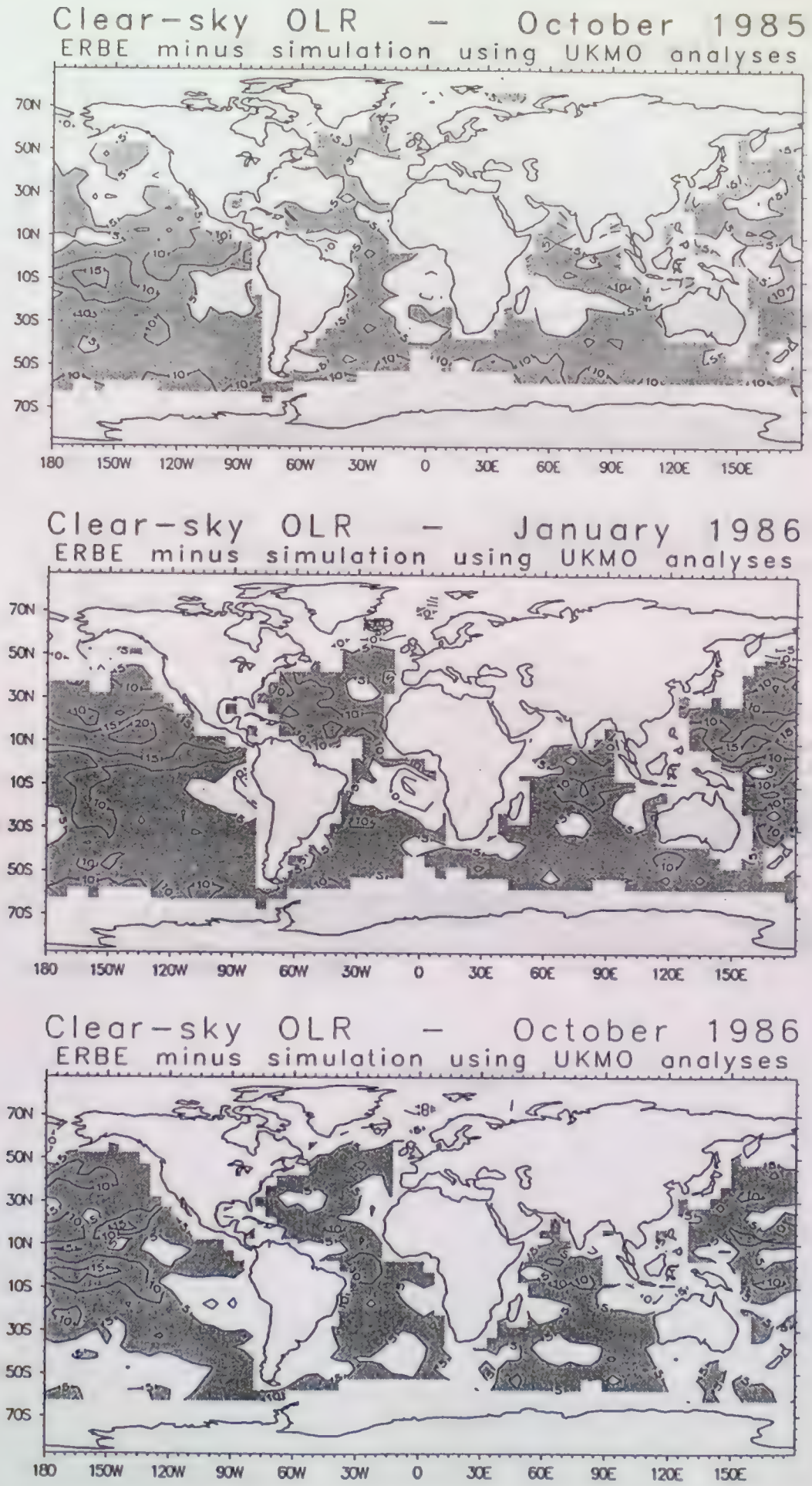

Figure 3 (continued)

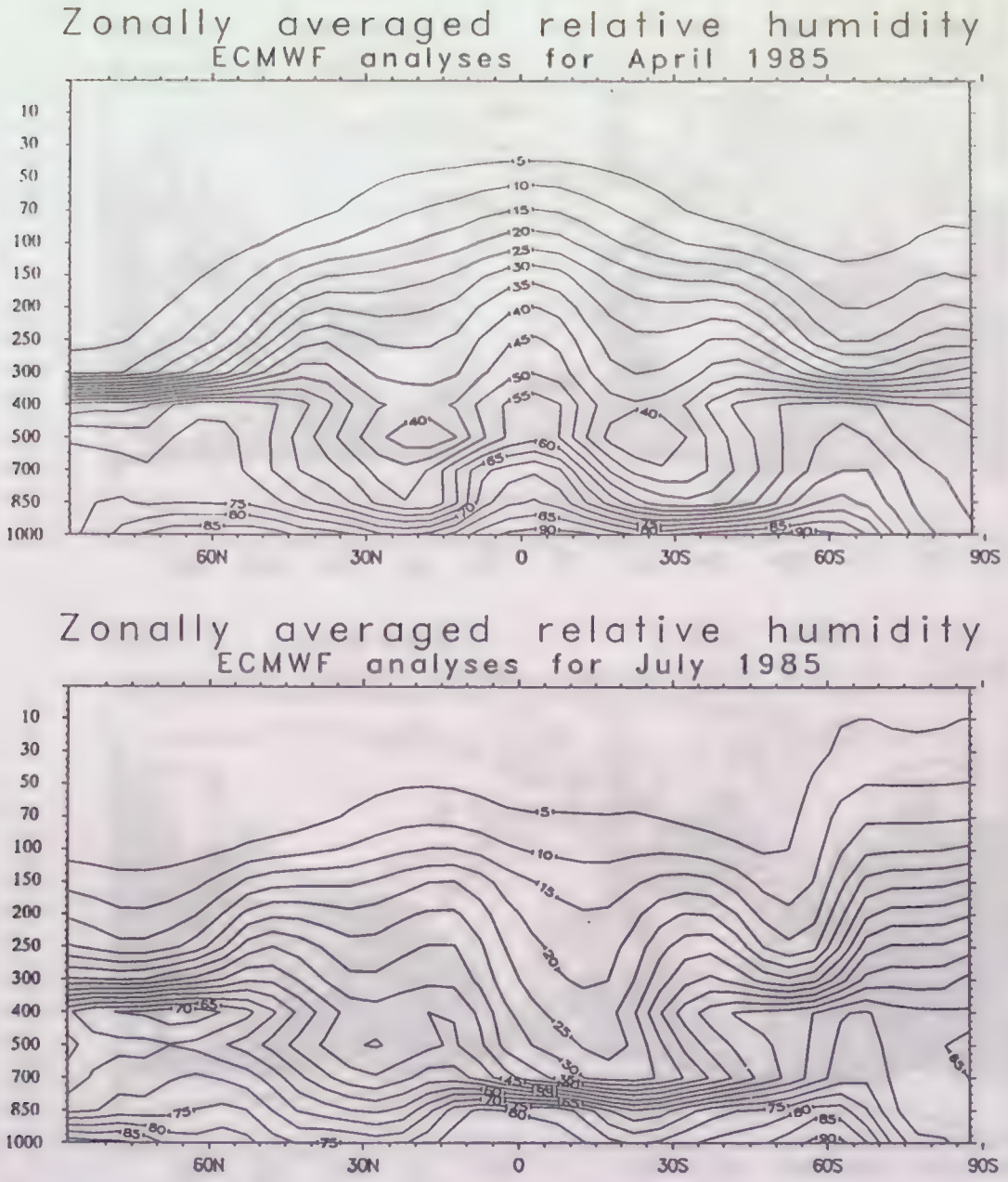
Zonally averaged relative humidity
ECMWF analyses for April 1985
10
30
50
70
100
150
200
250
300
400
500
700
850
1000
60N
30N
0
30S
60S
90S
Zonally averaged relative humidity
ECMWF analyses for July 1985
10
30
50
70
100
150
200
250
300
400
500
700
850
1000
60N
30N
0
30S
60S
90S

Figure 4

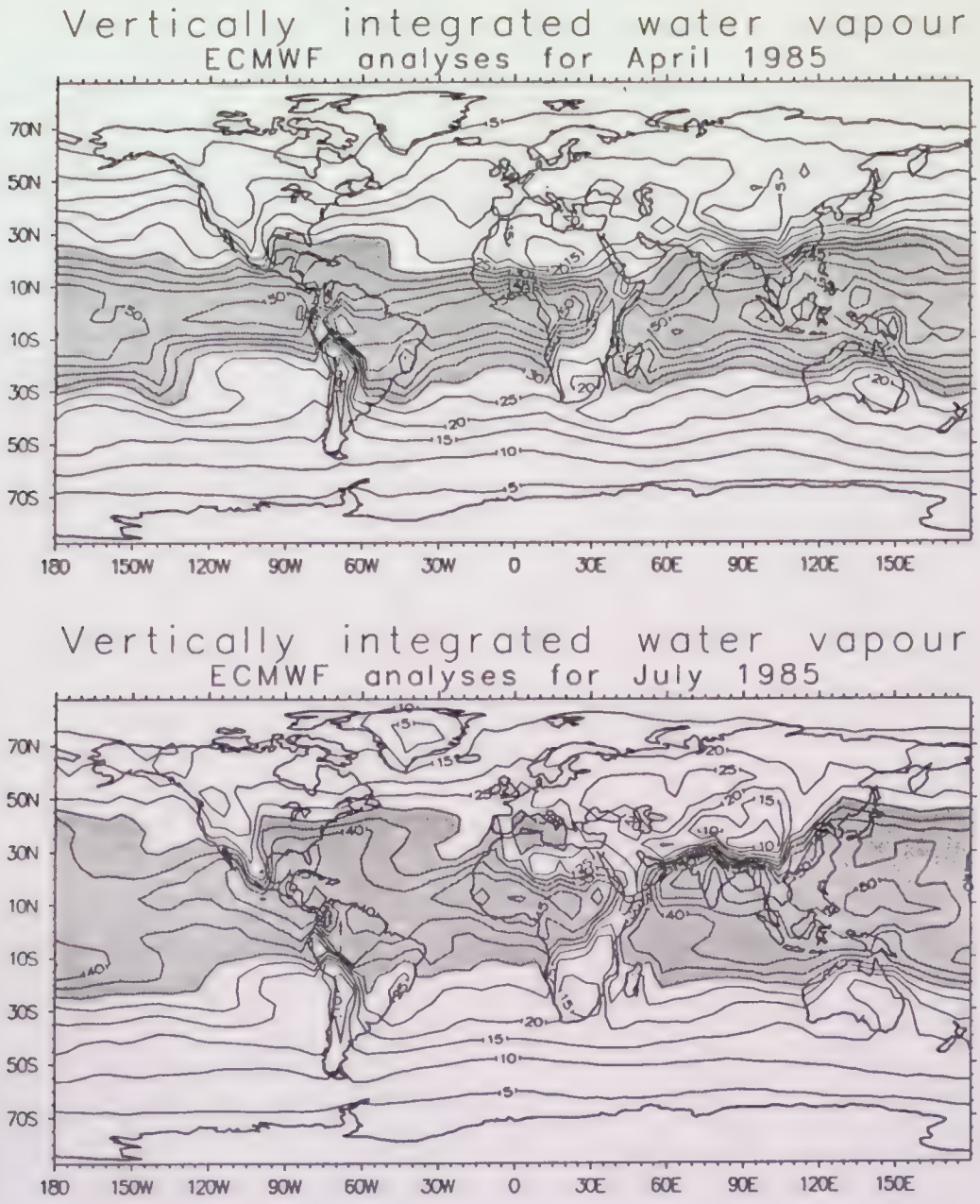
Vertically integrated water vapour
ECMWF analyses for April 1985
70N
50N
30N
10N
10S
30S
50S
70S
180
150W
120W
90W
60W
30W
0
30E
60E
90E
120E
150E
Vertically integrated water vapour
ECMWF analyses for July 1985
70N
50N
30N
10N
10S
30S
50S
70S
180
150W
120W
90W
60W
30W
0
30E
60E
90E
120E
150E

Figure 5

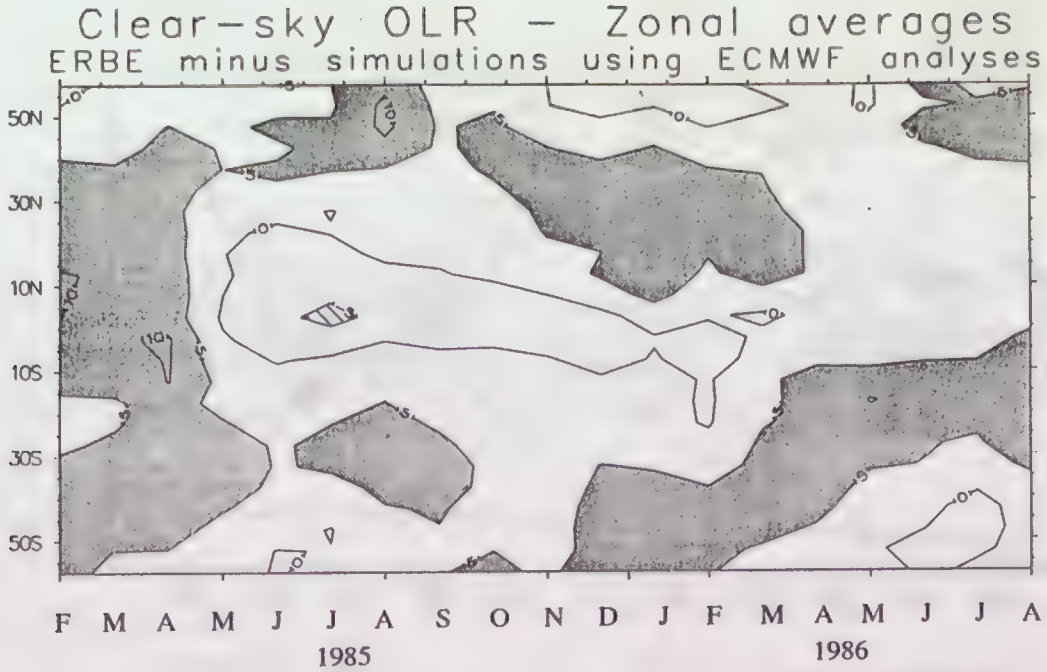
Clear-sky OLR - Zonal averages
ERBE minus simulations using ECMWF analyses
50N
30N
10N
10S
30S
50S
F M A M J J A S O N D J F M A M J J A
1985
1986

Figure 6

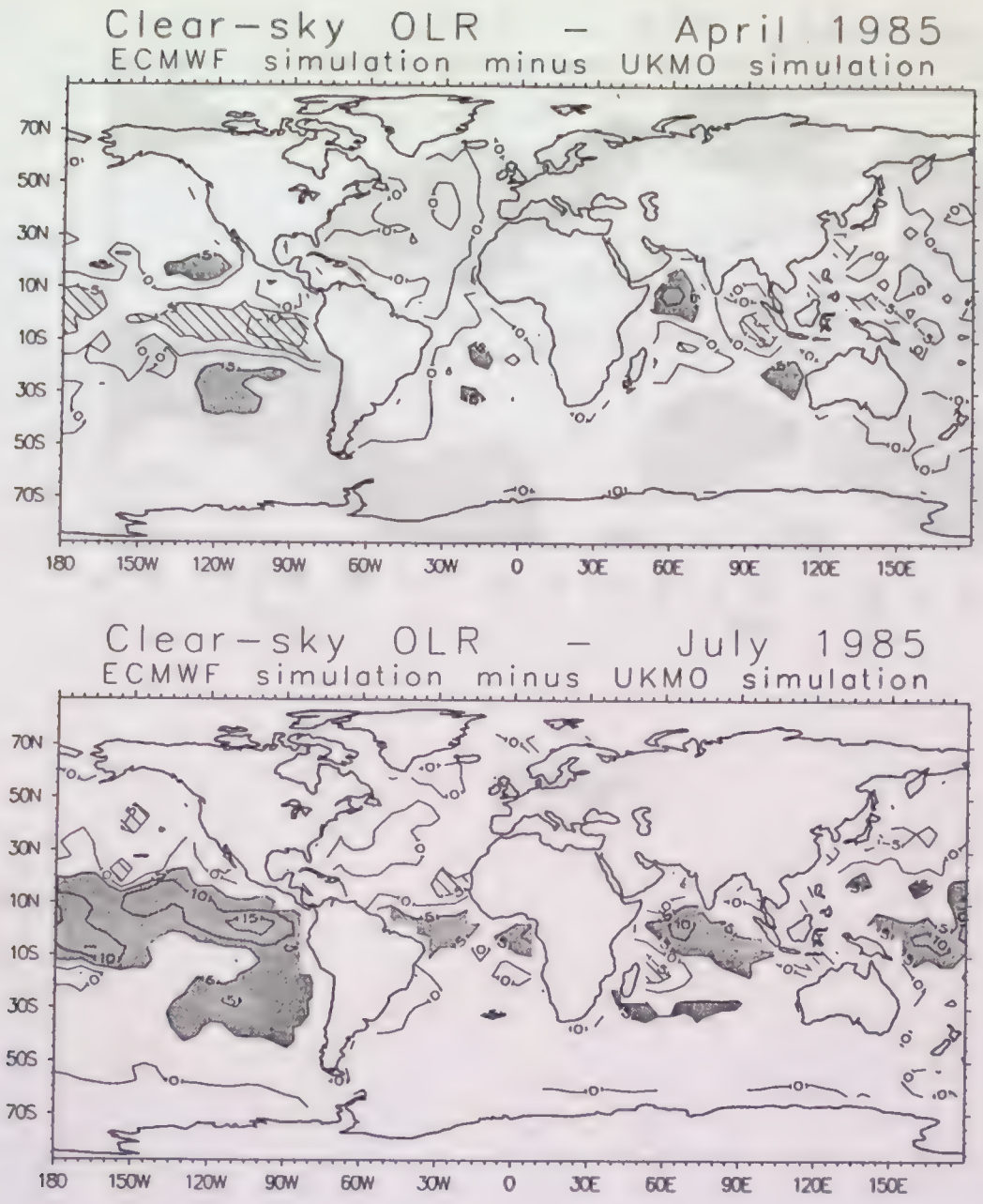
Clear-sky OLR – April 1985
ECMWF simulation minus UKMO simulation
70N
50N
30N
10N
10S
30S
50S
70S
180
150W
120W
90W
60W
30W
0
30E
60E
90E
120E
150E
Clear-sky OLR – July 1985
ECMWF simulation minus UKMO simulation
70N
50N
30N
10N
10S
30S
50S
70S
180
150W
120W
90W
60W
30W
0
30E
60E
90E
120E
150E

Figure 7

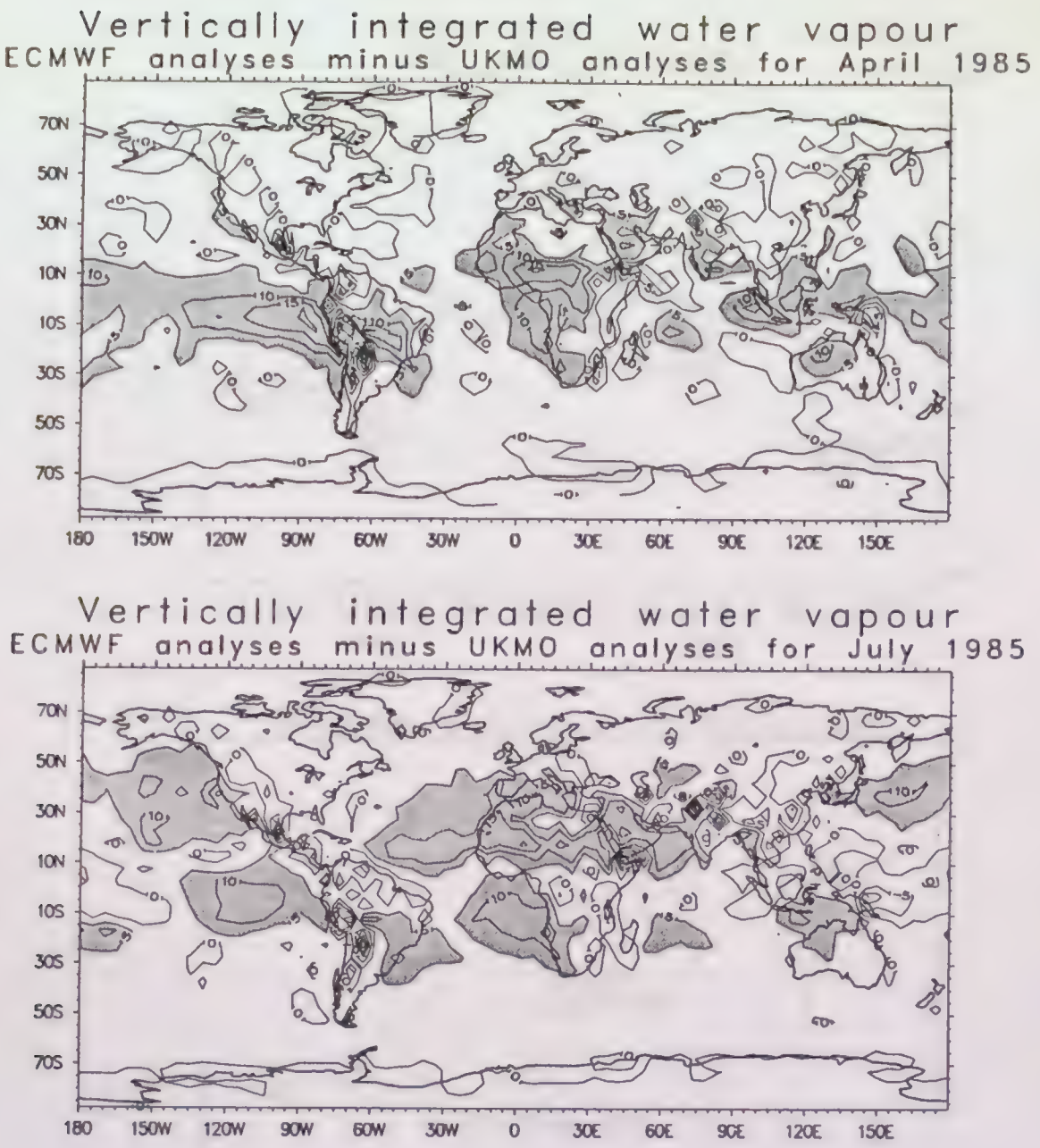

Figure 7 (continued)

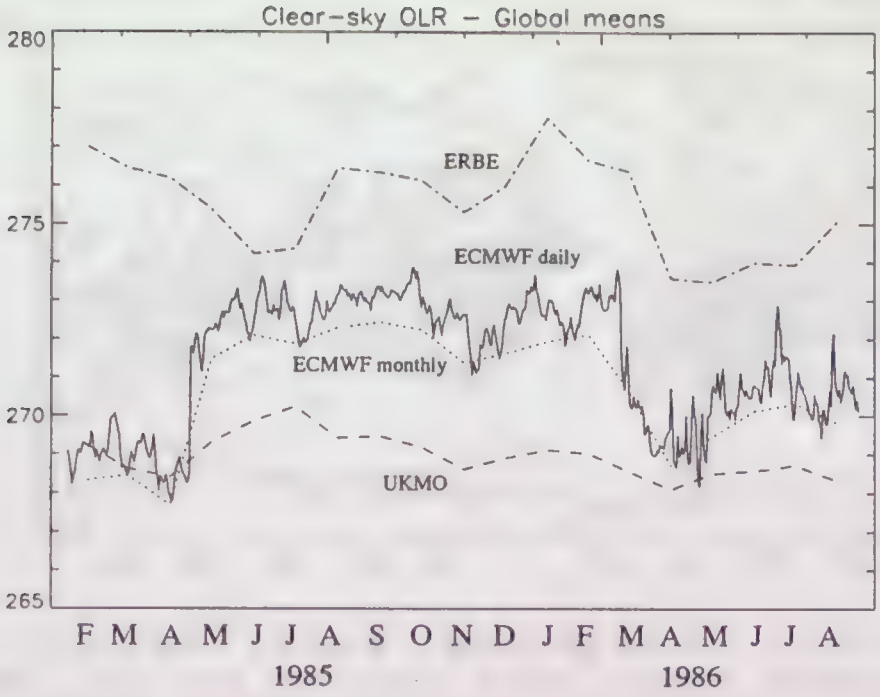
Clear–sky OLR – Global means
280
275
270
265
ERBE
ECMWF daily
ECMWF monthly
UKMO
F M A M J J A S O N D J F M A M J J A
1985
1986

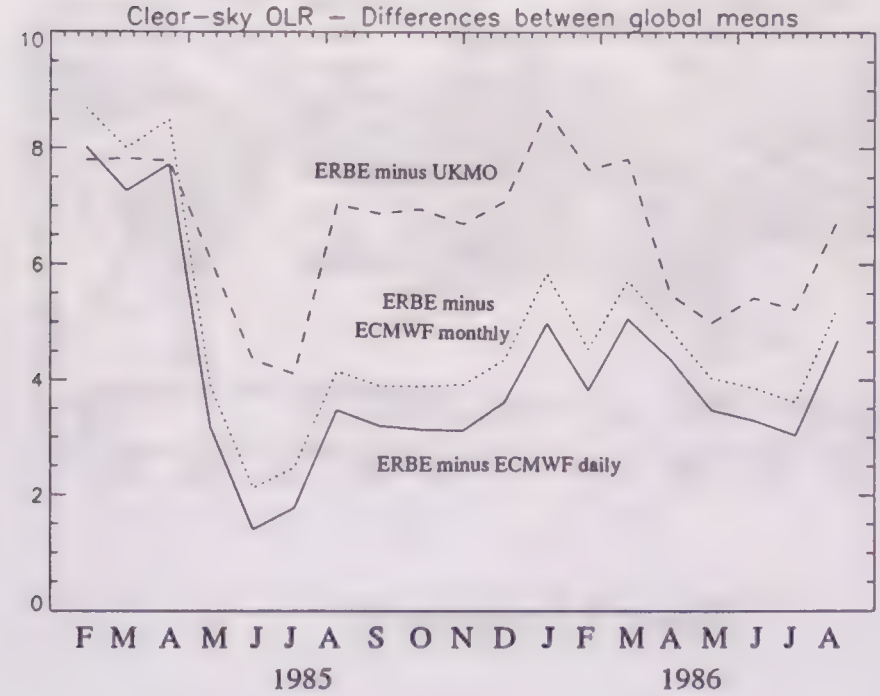
Clear–sky OLR – Differences between global means
10
8
6
4
2
0
ERBE minus UKMO
ERBE minus
ECMWF monthly
ERBE minus ECMWF daily
F M A M J J A S O N D J F M A M J J A
1985
1986

Figure 8

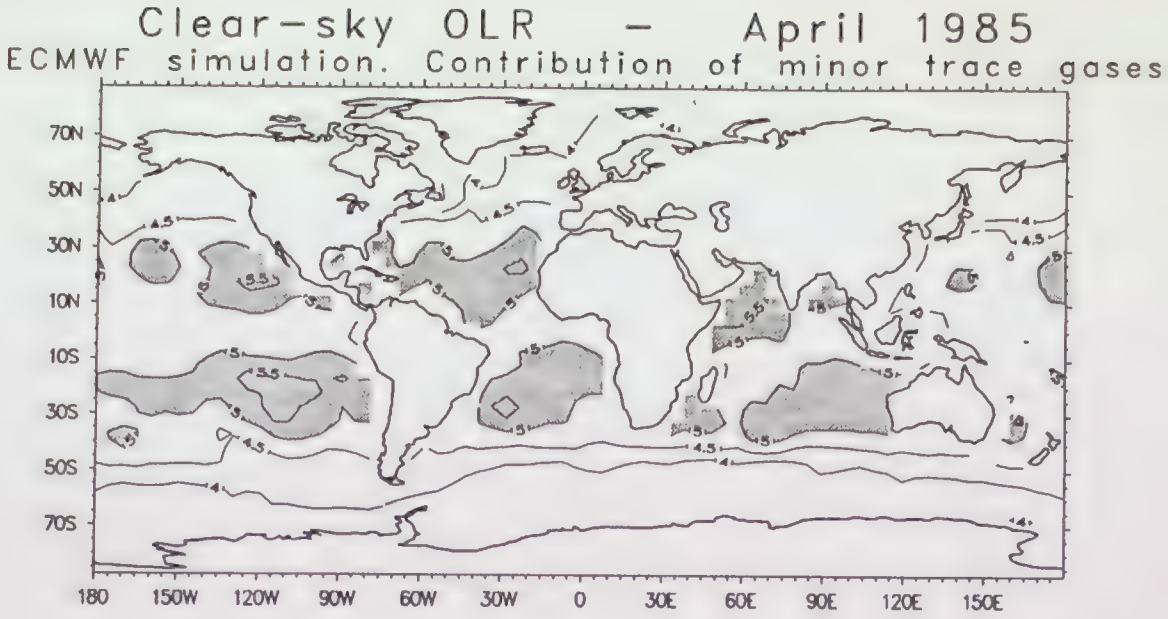
Clear-sky OLR - April 1985
ECMWF simulation. Contribution of minor trace gases
70N
50N
30N
10N
10S
30S
50S
70S
180
150W
120W
90W
60W
30W
0
30E
60E
90E
120E
150E

Figure 9

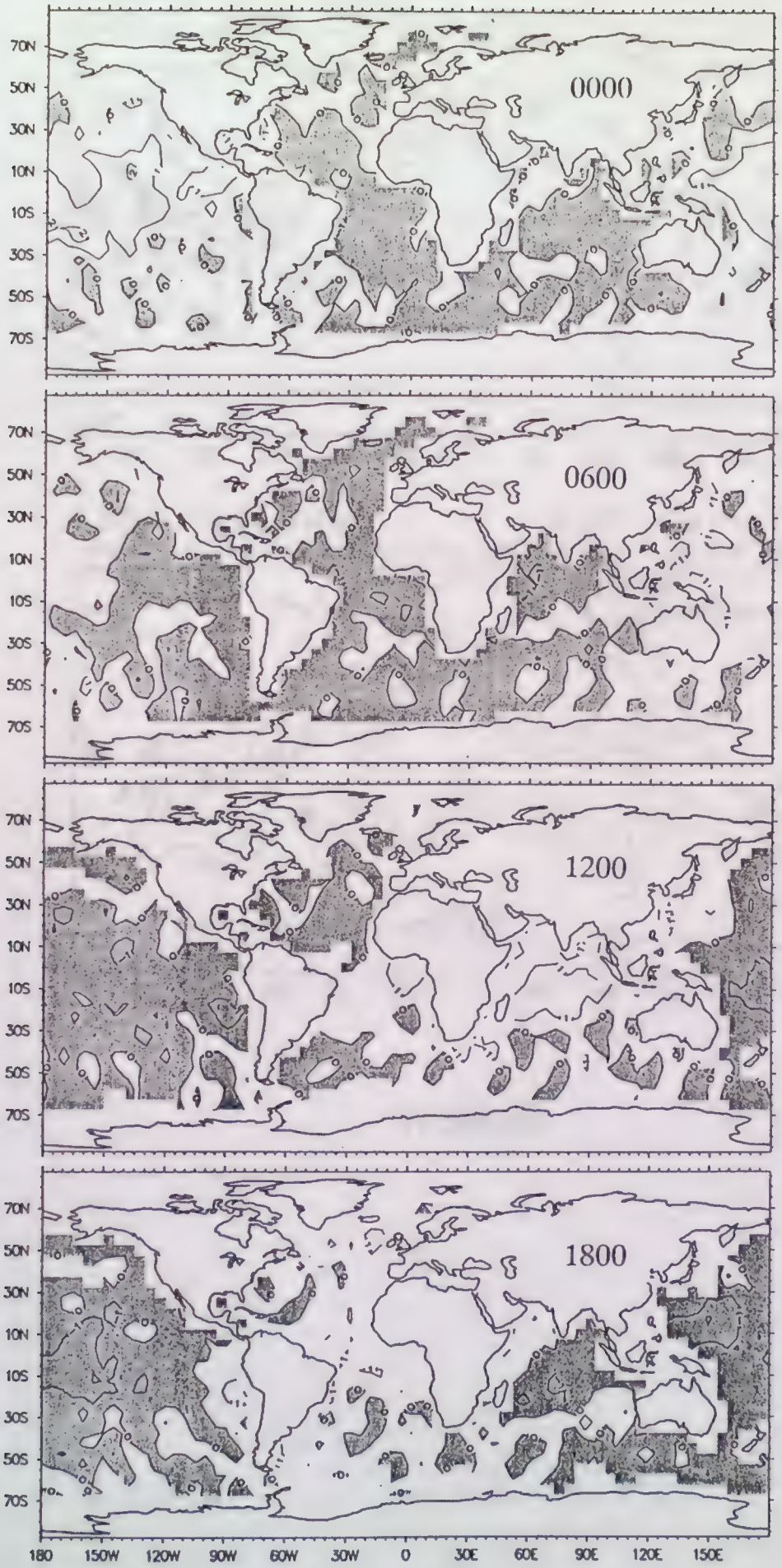
0000
0600
1200
1800
70N
50N
30N
10N
10S
30S
50S
70S
180
150W
120W
90W
60W
30W
0
30E
60E
90E
120E
150E

Figure 10

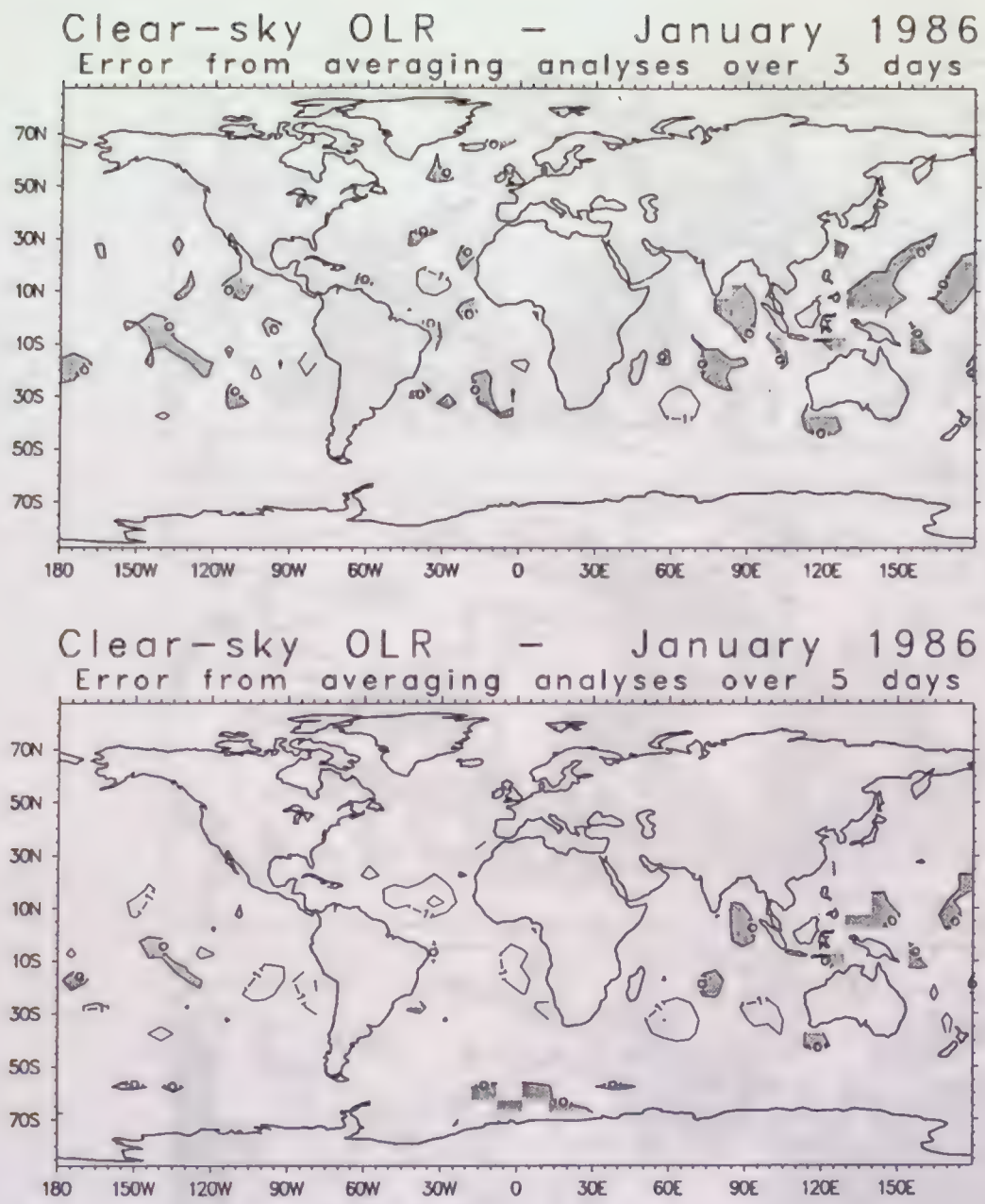
Clear-sky OLR - January 1986
Error from averaging analyses over 3 days
70N
50N
30N
10N
10S
30S
50S
70S
180
150W
120W
90W
60W
30W
0
30E
60E
90E
120E
150E
Clear-sky OLR - January 1986
Error from averaging analyses over 5 days
70N
50N
30N
10N
10S
30S
50S
70S
180
150W
120W
90W
60W
30W
0
30E
60E
90E
120E
150E

Figure 11

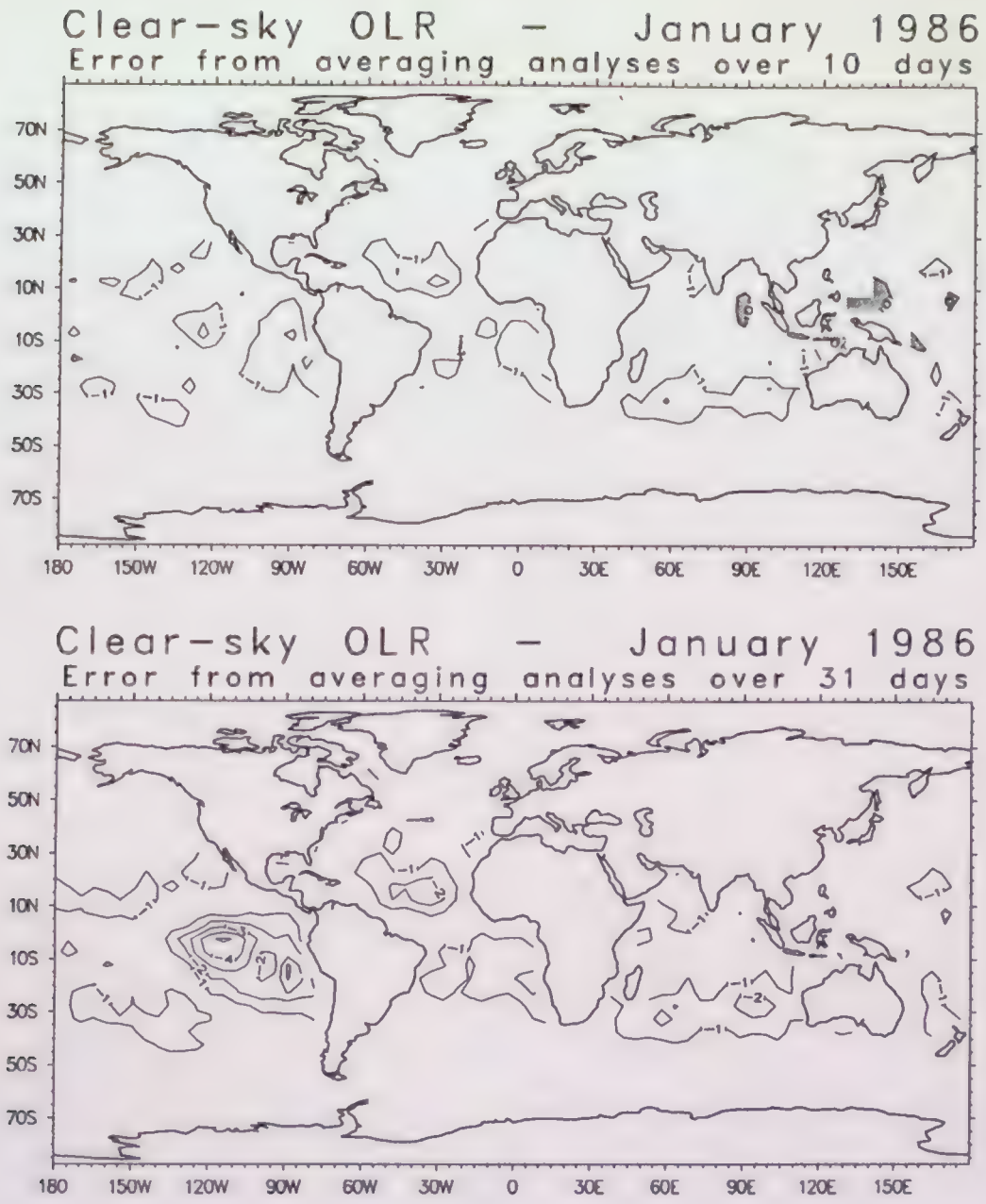

Figure 11 (continued)

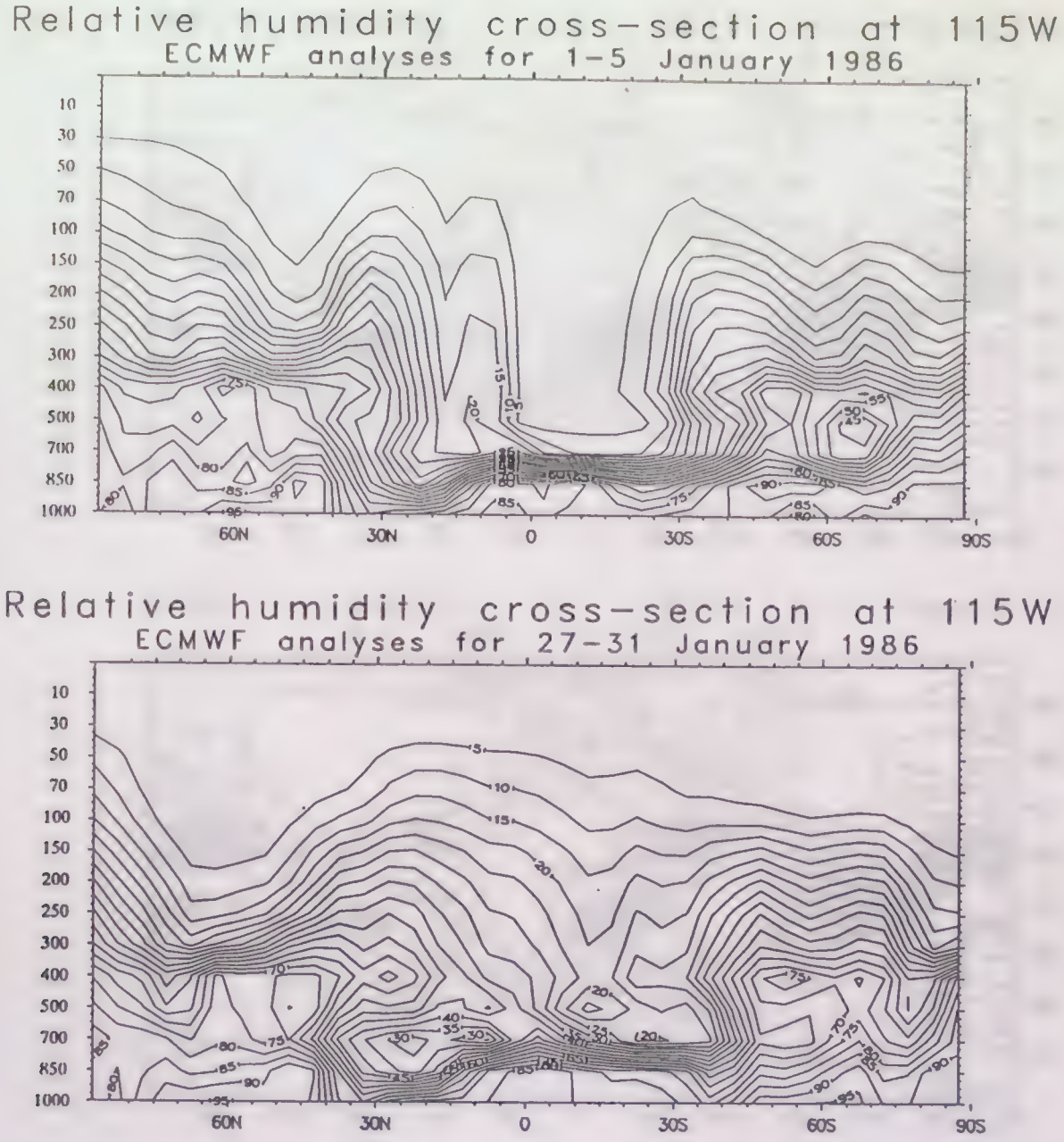
Relative humidity cross-section at 115W
ECMWF analyses for 1-5 January 1986
10
30
50
70
100
150
200
250
300
400
500
700
850
1000
60N
30N
0
30S
60S
90S
Relative humidity cross-section at 115W
ECMWF analyses for 27-31 January 1986
10
30
50
70
100
150
200
250
300
400
500
700
850
1000
60N
30N
0
30S
60S
90S

Figure 12

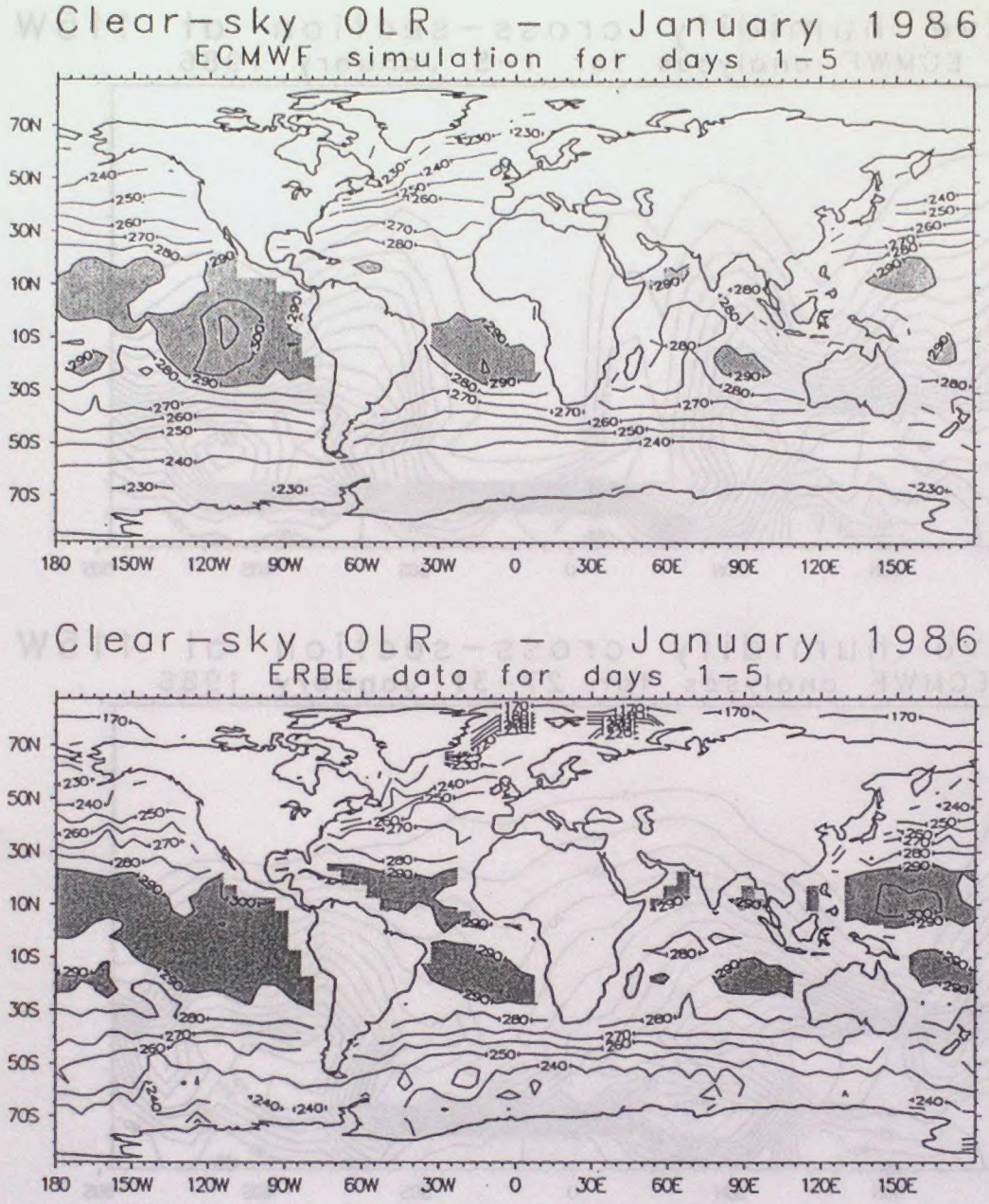
Clear-sky OLR – January 1986
ECMWF simulation for days 1-5
70N
50N
30N
10N
10S
30S
50S
70S
180 150W 120W 90W 60W 30W 0 30E 60E 90E 120E 150E
Clear-sky OLR – January 1986
ERBE data for days 1-5
70N
50N
30N
10N
10S
30S
50S
70S
180 150W 120W 90W 60W 30W 0 30E 60E 90E 120E 150E

Figure 13

CLIMATE RESEARCH TECHNICAL NOTES

CRTN 1	Oct 1990	Estimates of the sensitivity of climate to vegetation changes using the Penman-Monteith equation. P R Rowntree
CRTN 2	Oct 1990	An ocean general circulation model of the Indian Ocean for hindcasting studies. D J Carrington
CRTN 3	Oct 1990	Simulation of the tropical diurnal cycle in a climate model. D P Rowell
CRTN 4	Oct 1990	Low frequency variability of the oceans. C K Folland, A Colman, D E Parker and A Bevan
CRTN 5	Dec 1990	A comparison of 11-level General Circulation Model Simulations with observations in the East Sahel. K Maskell
CRTN 6	Dec 1990	Climate Change Prediction. J F B Mitchell and Qing-cun Zeng
CRTN 7	Jan 1991	Deforestation of Amazonia - modelling the effects of albedo change. M F Mylne and P R Rowntree
CRTN 8	Jan 1991	The role of observations in climate prediction and research. D J Carson
CRTN 9	Mar 1991	The greenhouse effect and its likely consequences for climate change. D J Carson
CRTN 10	Apr 1991	Use of wind stresses from operational N.W.P. models to force an O.G.C.M. of the Indian Ocean. D J Carrington
CRTN 11	Jun 1991	A new daily Central England Temperature series, 1772-1991. D E Parker, T P Legg and C K Folland
CRTN 12	Jul 1991	Causes and predictability of Sahel rainfall variability. D P Rowell, C K Folland, K Maskell, J A Owen, M N Ward
CRTN 13	Jul 1991	Modelling changes in climate due to enhanced CO_2, the role of atmospheric dynamics, cloud and moisture. C A Senior, J F B Mitchell, H Le Treut and Z-X Li

CLIMATE RESEARCH TECHNICAL NOTES

CRTN 14	Sep 1991	Sea temperature bucket models used to correct historical SST data in the Meteorological Office. C K Folland
CRTN 15	Aug 1991	Modelling climate change, and some potential effects on agriculture in the U.K. P R Rowntree, B A Callander and J Cochrane
CRTN 16	Aug 1991	The Boreal Forests and Climate G Thomas and P R Rowntree
CRTN 17	Aug 1991	Development of a Stratosphere-Troposphere Data Assimilation System. R Swinbank.
CRTN 18	Sep 1991	A study of asynchronous coupling using a simple climate model. M K Davey.
CRTN 19	Sep 1991	The Oceanic Carbon Cycle. N K Taylor
CRTN 20	Nov 1991	Worldwide ocean-atmosphere surface fields in Sahel wet and dry years using provisionally corrected surface wind data. M N Ward
CRTN 21	Dec 1991	Coupled tropical ocean global atmosphere models at the UKMO. M K Davey, C Gordon, S Ineson and S Lawrence
CRTN 22	Dec 1991	Empirical parameterisation of tropical ocean-atmosphere coupling. M Allen, M K Davey, D L T Anderson and P D Killworth
CRTN 23	Feb 1992	The temporal evolution of Equatorial Currents in the Indian Ocean D L T Anderson, D J Carrington, R A Corry and C Gordon
CRTN 24	Feb 1992	Stratospheric analyses provided by the U.K. Meteorological Office M J Bailey, A O'Neill and V D Pope
CRTN 25	Feb 1992	Modelling interannual variability in the Indian Ocean using momentum fluxes from the UKMO and ECMWF operational weather analyses. D L T Anderson and D J Carrington

CLIMATE RESEARCH TECHNICAL NOTES

CRTN 26	Mar 1992	A GCM simulation of the impact of Amazonian deforestation on climate using an improved canopy representation J Lean and P R Rowntree
CRTN 27	Mar 1992	The parameterization of rainfall interception in GCMs A J Dolman and D Gregory
CRTN 28	Jun 1992	Development of worldwide marine data eigenvectors since 1985 A W Colman
CRTN 29	Jun 1992	A tropical ocean model with reduced physics M K Davey
CRTN 30	Jun 1992	International Temperature Workshop, Boulder, Colorado, USA, 16 January 1992 Edited by D E Parker
CRTN 31	Jul 1992	Simulation of clear-sky outgoing longwave radiation over the oceans using operational analyses A Slingo and M J Webb